Knock-sideways by inducible ER retrieval reveals a novel extra-vacuolar function for *Plasmodium* PTEX component HSP101

Manuel A Fierro[1], Tahir Hussain[1], Liam J Campin[2] and Josh R Beck[1,2*]

[1]Department of Biomedical Sciences, Iowa State University, Ames, IA, 50011, USA

[2]Roy J. Carver Department of Biochemistry, Biophysics and Molecular Biology, Iowa State University, Ames, IA, 50011, USA

[*]Corresponding author: jrbeck@iastate.edu

Abstract

Malaria parasites uniquely depend on protein secretion for their obligate intracellular lifestyle but approaches for dissecting *Plasmodium* secreted protein functions are limited. We report knockER, a novel DiCre-mediated knock-sideways approach to sequester secreted proteins in the ER by inducible fusion with a KDEL ER-retrieval sequence. We show conditional ER sequestration of diverse proteins is not generally toxic, enabling loss-of-function studies. Taking advantage of the unique ability to redistribute secreted proteins from their terminal destination to the ER, we employed knockER to separate HSP101 function in protein export at the parasite vacuole from a recently proposed role in cargo recognition at the ER. Strikingly, while KDEL-fusion produced similar ER retrieval of both HSP101 and the translocon adaptor PTEX150, parasite growth and effector export were unaffected by HSP101 retention while ER retrieval of PTEX150 produced a lethal defect, indicating vacuolar HSP101 levels are uniquely maintained in excess. Moreover, vacuole depletion of HSP101 hypersensitized parasites to a destabilization tag that inhibits HSP101-PTEX complex formation but not to translational knockdown of the entire HSP101 pool, revealing vacuole-localized function does not fully account for HSP101 contribution to parasite fitness. These findings imply an important role for HSP101 in the ER distinct from the PTEX complex, suggesting a link between events that designate proteins for export during secretory pathway entry and their ultimate translocation into the host cell by PTEX. Collectively, our results establish knockER as a novel tool for dissecting secreted protein function with sub-compartmental resolution that should be widely amenable to genetically tractable eukaryotes.

35 **Significance**

36 Erythrocyte remodeling by *Plasmodium* exported proteins is central to parasite survival and
37 Malaria pathology. Effector proteins are transported from the parasite vacuole into the erythrocyte
38 through the PTEX translocon, a process powered by the AAA+ chaperone HSP101. Using a novel
39 approach to conditionally sequester secreted proteins in the ER (knockER), we provide evidence
40 for a distinct HSP101 activity in the ER upstream of the effector translocation site at the assembled
41 PTEX complex. Importantly, our results support a model where exported cargo is identified early
42 in the secretory pathway, possibly linking proteolytic maturation in the ER that licenses exported
43 proteins to recognition by PTEX. The knockER strategy is broadly applicable to functional
44 dissection of proteins that traverse the eukaryotic secretory pathway.

45 **Introduction**

46 Protein secretion is a fundamental biological process of all living cells. In eukaryotes this
47 is accomplished by a dedicated secretory pathway that begins with import into the Endoplasmic
48 Reticulum (ER) for initial folding and post-translational modification, followed by sorting in the
49 Golgi and post-Golgi compartments. As an obligate intracellular parasite, secreted proteins play
50 a critical role in the biology of the malaria parasite, *Plasmodium*. Through the secretory pathway,
51 proteins are trafficked into both the plasma membrane and several organelles, including a relict
52 plastid called the apicoplast that is critical for parasite metabolism (1, 2). During schizogony,
53 another subset of proteins is packaged into several distinct secretory organelles that are
54 subsequently discharged to facilitate host cell attachment and penetration (3). Invagination of the
55 host membrane by the parasite during invasion generates an intracellular microenvironment
56 called the parasitophorous vacuole (PV) which forms the interface for host-parasite interactions
57 (4). Resident PV proteins secreted into the vacuole perform critical functions at this interface,
58 including nutrient/waste exchange and protein export (5). The later process enables parasites to
59 deploy a battery of secreted effector proteins across the PV membrane (PVM) and into the host
60 compartment, dramatically remodeling the erythrocyte to meet nutritional demands and avoid host
61 defenses (6, 7). Remarkably, it is estimated that up to 10% of the parasite genome is devoted to
62 encoding exported effectors, further highlighting the central importance of protein secretion to this
63 parasitic lifestyle (8-12).

64 As with other eukaryotes, entry into the malaria parasite secretory pathway generally
65 begins with co-translational import of proteins containing a signal peptide or transmembrane
66 domain(s) into the ER via the Sec61 complex, followed by sorting from the Golgi to internal
67 compartments, the PV or beyond into the host (13). ER-resident proteins that escape the ER via
68 bulk flow in COPII vesicles are returned to the ER in COPI vesicles by ERD2 surveillance, which
69 binds a C-terminal retrieval sequence ("KDEL" and variants) in the *cis* Golgi and releases it in the
70 ER in a pH-dependent manner (14-16). Similar to other eukaryotes, ER retention of secreted

71 reporters or chimeric proteins can be achieved in *Plasmodium spp.* by a C-terminal KDEL or
72 functional variants (17-22).

73 In this present work, we developed and characterized a novel DiCre-based knock-
74 sideways tool called knockER that enables conditional fusion of KDEL to the C-terminus of
75 secreted proteins, subjecting the target protein to ERD2 surveillance in the *cis* Golgi to cause its
76 retrieval to the ER. Using this approach, we show successful conditional retrieval of five
77 endogenous *Plasmodium* proteins (ClpB1, RON6, EXP2, PTEX150 and HSP101) that traffic
78 through the ER to diverse compartments including the apicoplast, rhoptries, dense granules, and
79 the PV. Importantly, conditional ER retrieval of both highly expressed reporters and endogenously
80 tagged proteins does not generally impact fitness, indicating knockER-mediated phenotypes are
81 not the indirect result of an integrated stress response, thus making this system suitable for protein
82 loss-of-function studies. Taking advantage of the unique ability to redistribute secreted proteins
83 from their terminal destination to the ER, we employed knockER to interrogate a recently
84 proposed ER function for the PTEX translocon component HSP101 in addition to its role in the
85 PV (23). We reveal a surprising insensitivity to ER retrieval of HSP101 in contrast to the other
86 PTEX components, indicating HSP101 is maintained in excess in the PV. Interestingly,
87 redistribution of HSP101 from the PV to the ER hypersensitized parasites to a post-translational
88 destabilization tag that disrupts HSP101 interaction with PTEX but not to translational knockdown,
89 providing support for an HSP101 function in the early secretory pathway in addition to its role in
90 protein translocation across the PVM in the assembled PTEX complex (24-26). These results
91 establish knockER as a novel tool to study eukaryotic secreted proteins and provide the first
92 functional evidence for an extra-vacuolar role for HSP101, highlighting the unique ability of
93 knockER to resolve function between compartments for dually localized proteins.

94

95 **Results**

96 **Conditional ER retrieval of a secreted reporter does not impact parasite fitness**

97 To facilitate conditional ER retrieval of a protein of interest, we designed a strategy based
98 on the dimerizable Cre recombinase (DiCre) system (27, 28) where a gene of interest is C-
99 terminally fused to a 3xFLAG tag and a stop codon flanked by *loxP* sequences imbedded in small
100 introns (29). Activation of DiCre by rapamycin results in excision of the loxP-intervening sequence,
101 removing the 3xFLAG tag and stop codon and bringing into frame a 3xHA tag followed by the ER-
102 retention sequence KDEL and a stop codon (Figure 1A). While the ER plays a crucial role in
103 quality control and is sensitive to added stress, several previous studies have exogenously
104 expressed various KDEL or SDEL fusion proteins in *P. falciparum* and *P. berghei* without apparent
105 impact on parasite fitness (19, 30-37). To directly ascertain whether ER retrieval of a highly
106 expressed secreted protein impacted parasite fitness, we first appended the knockER system to
107 an mNeonGreen (mNG) reporter and fused this to the *exp2* 5' UTR and signal peptide, enabling
108 expression from the strong *exp2* promoter and entry into the ER followed by default secretion into
109 the PV (38-40). This assembly was placed under control of the anhydrotetracycline (aTc)-
110 responsive TetR-DOZI-aptamers system to prevent expression until aTc is present in the culture
111 (Figure 1A) (41, 42). To combine the Bxb1 integrase system with DiCre, we first introduced a
112 DiCre expression cassette at the benign *pfs47* locus (28) in the *P. falciparum* NF54^{attB} strain (43)
113 (Figure S1) and then integrated the mNG-knockER reporter construct at the *attB* site in the *cg6*
114 locus on chromosome 6 in this NF54$^{attB\text{-}DiCre}$ line.
115 Upon treatment with rapamycin, parasites efficiently excised the knockER cassette (kER),
116 resulting in the expected tag switching from FLAG to HA (Figure 1B,C). Examination of DMSO
117 vehicle-treated parasites by live microscopy showed a peripheral mNG signal, consistent with
118 secretion to the PV (Figure 1D). In contrast, following treatment with rapamycin the mNG signal
119 was dramatically altered to an intracellular, perinuclear pattern that co-localized with ER Tracker,
120 confirming retention in the ER (Figure 1D). Quantification of the distribution of mNG fluorescence
121 between the parasite periphery and interior showed substantial re-localization following KDEL
122 fusion, indicating robust retrieval by ERD2 (Figure 1E, mean % internal mNG 42.54 ± 6.0% in

123 DMSO vs 84.66 ± 6.9% in Rap). Importantly, ER retention of mNG had no impact on parasite
124 growth (Figure 1F) showing that knockER can successfully retrieve a secreted reporter to the ER
125 without impacting parasite fitness.
126
127 **knockER reveals Golgi-dependent trafficking and essential apicoplast functionality of**
128 **ClpB1**
129 Next, we applied knockER to an endogenous gene for conditional loss-of-function
130 mutagenesis. We choose ClpB1, a poorly characterized, nuclear-encoded AAA+ class 1
131 Clp/HSP100 chaperone that is targeted to the apicoplast (44). As apicoplast ablation can be
132 chemically rescued with isopentenyl pyrophosphate (IPP) (45), we reasoned that IPP
133 supplementation would provide a simple validation that any loss of parasite fitness is a direct
134 effect of sequestering ClpB1 away from its site of action and not an indirect result of ER stress.
135 ClpB1 contains both a signal peptide for ER entry and a transit peptide for apicoplast targeting
136 and localization of ClpB1 to this organelle was previously confirmed by both microscopy and
137 proteomic analyses (36, 44). Using CRISPR/Cas9 editing, we fused mNG to the C-terminus of
138 ClpB1 followed by the kER cassette (Figure 2A). As expected, IFA demonstrated co-localization
139 with the apicoplast marker ACP1, confirming ClpB1 localization to this organelle (Figure 2B).
140 Treatment with rapamycin resulted in efficient excision (Figure 2C) and switching to the 3xHA-
141 KDEL tag produced a shift in migration by Western blot consistent with an increase in molecular
142 weight of ~14 kDa in the rapamycin treated samples, indicating that the N-terminal transit peptide
143 (residues 24-152, 13.9 kDa) is no longer cleaved in the ClpB1-KDEL fusion (Figure 2C,D). Since
144 this maturation event takes place in the apicoplast (46), this suggested that ClpB1 was no longer
145 being trafficked to this organelle. Indeed, live microscopy showed a dramatic re-localization of
146 mNG from puncta to a perinuclear distribution that co-localized with ER Tracker, indicative of
147 successful ER retrieval (Figure 2E).

148 While its functional importance has not been directly tested, ClpB1 is expected to be
149 essential for blood-stage survival based on saturating insertional mutagenesis in *P. falciparum*
150 and pooled knockout screens in *P. berghei* (47, 48). Indeed, ER retention of ClpB1 was lethal and
151 resulted in delayed parasite death (Figure 2F), consistent with an essential role in the apicoplast
152 (49, 50). Moreover, supplementation with IPP fully rescued parasite growth, confirming the
153 observed phenotype was apicoplast-specific and not due to a disruption of ER homeostasis
154 following ClpB1 retention (Figure 2F). Rapamycin-treated parasites supplemented with IPP
155 showed dispersed, vesicular ACP1 signal consistent with plastid disruption, further indicating
156 ClpB1 is required for apicoplast maintenance (Figure 2G). Taken together, these results show for
157 the first time that ClpB1 is an indispensable component of the apicoplast machinery and illustrate
158 that knockER can be used for protein loss-of-function studies in *P. falciparum*.
159

160 **knockER induces ER retrieval of rhoptry proteins**

161 Having demonstrated that knockER is suitable to generate loss-of-function phenotypes by
162 protein mis-localization to the ER, we next tested this knock-sideways approach on an expanded
163 set of endogenous soluble and membrane proteins that traffic through the secretory pathway to
164 diverse destinations, including secretory organelles and the PV/PVM. We began by attempting to
165 retrieve RON6, a soluble rhoptry-neck protein that is injected into the PV during invasion (Figure
166 S2A,B). Attempts predating CRISPR technology to disrupt *Pfron6* or truncate its Cysteine-rich C-
167 terminus were unsuccessful (51). More recently, saturating transposon mutagenesis in *P.*
168 *falciparum* recovered a single insertion within an intron (47) expected to generate a truncation at
169 residue 713 of 950, leaving most of the protein intact (Figure S2A). Curiously, RON6 orthologs in
170 rodent malaria parasites lack the cysteine-rich region which accounts for the C-terminal ~23% of
171 *P. falciparum* RON6, roughly corresponding to the truncated region in the insertional mutant. As
172 RON6 was not targeted in the PlasmoGEM data set, its suspected essentiality remains uncertain
173 (48). To directly test the importance of RON6, we generated RON6-kER parasites, which

174 underwent efficient excision upon rapamycin treatment (Figure S2C,D). Rapamycin treatment
175 resulted in re-localization of RON6 from the rhoptries to the ER and produced a minor but
176 reproducible growth defect (Figure S2E,F). These results suggest that RON6 is dispensable in
177 the blood stage, although we cannot exclude the possibility that small amounts of RON6-KDEL
178 may escape ERD2 surveillance at levels sufficient to mediate a critical function. Additionally, the
179 minor fitness defect that results from RON6-KDEL fusion could be the indirect result of modest
180 ER stress induced by RON6 retention. Nonetheless, these findings clearly demonstrate that
181 knockER efficiently retrieves secretory proteins synthesized during the brief period of merozoite
182 formation at the terminal phase of intraerythrocytic development.
183

184 **ER retention of EXP2 produces a lethal defect independent to loss of PVM transport**
185 **function**

186 Having successfully retained several soluble proteins in the ER using knockER, we next
187 tested conditional retrieval of a membrane protein. Solute permeation across the PVM is mediated
188 by a nutrient-permeable channel (52, 53) whose identity was recently tied to EXP2, a PVM protein
189 broadly conserved among vacuole-dwelling apicomplexans (54, 55). EXP2 contains a signal
190 peptide followed by an N-terminal amphipathic helix and oligomerizes to form a heptameric pore
191 in the PVM (26, 56, 57). It is currently unknown how pore formation is specifically constrained to
192 the PVM to avoid perforating other membranes along the secretory pathway or the parasite
193 plasma membrane. While not structurally homologous to the EXP2 pore, bacterial α-helical pore
194 forming toxins are functionally analogous and provide a possible model for EXP2 pore formation.
195 These proteins are typically maintained in a monomeric state that shields a membrane-spanning
196 amphipathic helix, enabling soluble trafficking until contact with components of a target membrane
197 triggers conformational rearrangement, leading to membrane insertion and oligomerization (58).

198 If EXP2 traffics in a similar configuration, then its C-terminus will enter the secretory
199 pathway lumen and be sensitive to ER-retrieval by KDEL fusion. Indeed, we endogenously tagged

200 EXP2 with a version of the kER cassette lacking mNG and found that KDEL fusion disrupted
201 EXP2 trafficking to the PV and resulted in ER retention, confirming its C-terminus resides in the
202 secretory pathway lumen (Figure 3A-D and S3). Notably, ER retrieval of EXP2 caused rapid
203 parasite death at earlier time points than post-transcriptional conditional knockdown of EXP2 (54,
204 59) (Figure 3E). To test whether this was solely due to loss of EXP2 transport functions in the PV
205 and not an indirect result of retaining EXP2 in the ER, we generated parasites expressing a
206 second copy of EXP2-mNG-kER from the *attB* locus under the control of its own promoter, leaving
207 the endogenous EXP2 locus unaltered (Figure S3). Retrieval of this second copy of EXP2 to the
208 ER also resulted in parasite death, indicating that EXP2 retention in the ER is toxic independent
209 of compromised transport functions at the PVM (Figure 3F,G). In contrast, ER retrieval of a second
210 copy of EXP2 lacking the amphipathic helix did not cause parasite death (Figure 3H,I and S3). As
211 expected, prior to KDEL fusion the ΔTM version of EXP2 localized to the PV and the digestive
212 vacuole (due to endocytosis of PV proteins along with RBC cytosol); surprisingly, however, some
213 cells also showed EXP2ΔTM-mNG export into the RBC cytoplasm (arrow, Figure 3H). The
214 requirement for the amphipathic helix in EXP2-kER toxicity suggests that increasing EXP2 dwell
215 time in the early secretory pathway may trigger an unfolded protein response or cause aberrant
216 EXP2 pore formation in the ER membrane. Thus, this may provide a new tool for studying EXP2
217 pore formation but also indicates knockER may not be appropriate for loss-of-function studies of
218 certain membrane proteins.
219

220 **ER retention of PTEX150 but not HSP101 results in loss of PTEX function *in vitro***

221 In malaria parasites, the nutrient-permeable channel has been additionally functionalized
222 by the flange-like adaptor PTEX150 which docks the AAA+ chaperone HSP101 onto EXP2 to
223 form the *Plasmodium* Translocon of Exported proteins (PTEX), transforming EXP2 into a protein-
224 conducting pore to translocate effector proteins across the PVM and into the erythrocyte (24-26,
225 54, 60). Interestingly, HSP101 shows a dual localization to both the PV and the ER as opposed

226 to EXP2 and PTEX150, which localize exclusively to the PV and form a sub-complex independent
227 of HSP101 (23, 35, 40, 61). We verified this unique ER localization of HSP101 by protease
228 protection assays in parasite lines expressing fluorescently tagged versions of each PTEX core
229 component, confirming an internal, perinuclear pool of HSP101 but not EXP2 or PTEX150 (Figure
230 S4). This arrangement suggests that in addition to powering translocation in the assembled PTEX
231 complex, HSP101 may also function upstream of the vacuole, possibly initiating cargo selection
232 early in the secretory pathway (23). While several HSP101 conditional knockdown (23, 25) or
233 inactivation (24) strategies have demonstrated an essential role in protein export, it is difficult to
234 resolve distinct compartmental functions with these mutants given that they impact the total
235 protein pool and have no sub-compartmental resolution. In contrast, knockER provides a strategy
236 to resolve potential HSP101 functions across distinct compartments by redistributing the target
237 protein pool from the PV to the ER.

238 In an attempt to separate HSP101 ER function from its role in the PV, we generated a kER
239 fusion to the endogenous copy of HSP101. In parallel, we also generated a PTEX150-kER line,
240 reasoning that since HSP101 and PTEX150 have similar expression timing and are exclusively
241 involved in protein export but not nutrient uptake (54), PTEX150 would provide a control for
242 knockER inactivation of PTEX activity independent of ER function. As expected, the PTEX150-
243 KDEL fusion was efficiently retrieved to the ER, producing a lethal growth defect and
244 accompanying block in protein export (Figure 4A-E), similar to *glmS* ribozyme-mediated
245 knockdown of PTEX150 (25). Importantly, ER retention of a second copy of PTEX150-kER in
246 parasites where the endogenous PTEX150 locus was unmodified did not impact growth,
247 demonstrating that the phenotype observed upon ER retention of the endogenously tagged
248 protein is a direct result of functional disruption of PTEX150 (Figure S5A-D).

249 Unexpectedly, although rapamycin-induced HSP101-KDEL fusion increased ER
250 localization similar to PTEX150 (Figure 4F-H), parasite growth was completely unaffected and
251 protein export was not detectibly impacted (Figure 4I,J), sharply contrasting with the lethal export

252 defect observed with HSP101 depletion or inactivation mutants (23-25). Indeed, HSP101-kER
253 parasites could be cultured indefinitely following excision and displayed sustained ER retention
254 of HSP101 (Figure 4H and S5E,F, mean Rap internal HSP101 58.82±9.58% at 24 hours vs
255 54.82±9.84% at 7 days). As an orthogonal approach to monitor protein redistribution by KDEL
256 fusion, we released infected RBCs with saponin to permeabilize the PVM and quantified
257 fluorescence via flow cytometry with or without proteinase K treatment. Again, we observed an
258 increase in protected fluorescence following rapamycin treatment, consistent with redistribution
259 of HSP101 to the ER (Figure S5G). Importantly, PCR and Western blot indicated that rapamycin-
260 treated parasites had undergone complete excision with the pre-excised FLAG-tagged version of
261 HSP101 no longer detectible (Figure 4F,G). Furthermore, both the mNG-FLAG and mNG-HA-
262 KDEL tagged versions of HSP101 migrated as a single band at the expected size for the full-
263 length fusion proteins with no apparent breakdown products, ensuring that the mNG signal
264 distribution observed by live microscopy reflected an intact HSP101 fusion (Figure 4G and S8B).
265 While a large fraction of PTEX150 and HSP101 was clearly ER-retained following
266 knockER induction, some peripheral signal was still apparent after rapamycin treatment (Figure
267 4C,H). To determine whether the observed phenotypic differences between HSP101 and
268 PTEX150 were due to a difference in sensitivity to ERD2 surveillance, we quantified the internal
269 mNG fluorescence signal in HSP101- and PTEX150-kER parasites following KDEL fusion. In
270 synchronized parasites, a similar increase in internal signal was observed in both lines at 24 hours
271 post Rap treatment (Figure S5E, mean Rap internal HSP101 58.82±9.58% vs 56.32±18.56% for
272 PTEX150). Since a comparison could not be made with PTEX150-kER parasites at 7 days due
273 to parasite death by the second cycle follow excision, we compared HSP101-kER parasites with
274 PTEX150-kER^{attB} control parasites 7 days after excision and again observed a comparable
275 internal signal redistribution (Figure S5F, mean Rap internal HSP101 54.82±9.84% vs
276 61.75±16.27% for PTEX150 at 7 days). As differential ER retrieval cannot account for parasite

277 insensitivity to HSP101-kER, these results indicate vacuolar HSP101 levels are uniquely
278 maintained in excess from what is required for PTEX function at the PVM.
279
280 **ER retention of HSP101 is lethal *in vivo***
281 Lack of observable phenotypes *in vitro* can sometimes be masked by the rich resources
282 available in culture conditions (62, 63). Furthermore, many exported effectors critical for survival
283 in the vertebrate host are dispensable in culture (12) and export-related defects that escape
284 detection *in vitro* can be exposed *in vivo* where parasites have to contend with host defenses and
285 more limited nutrient access (64, 65). To determine if ER retention of HSP101 was similarly
286 tolerated *in vivo*, we tagged HSP101 and PTEX150 with kER in a *P. berghei* rodent malaria DiCre
287 parasite and evaluated the impact of ER retrieval on parasite survival during mouse infection
288 (Figure S6A). Similar to *P. falciparum* knockER mutants, rapamycin treatment *ex vivo* produced
289 efficient excision and ER retrieval of PbPTEX150 and PbHSP101 (Figure 5A-D). After overnight
290 *ex vivo* culture to allow for tag switching, equal numbers of DMSO or rapamycin treated parasites
291 were IV injected into naïve mice. Strikingly, while DMSO controls became patent by day two post-
292 injection, neither KDEL-fused PbPTEX150 or PbHSP101 parasites appeared over the course of
293 10 days before the experiment was terminated (Figure 5E,F and S6B). That ER-retrieval of
294 PbHSP101 compromises function sufficiently to prohibit survival in the mammalian host reinforces
295 the established critical role of HSP101 in the PV and indicates that KDEL-mediated depletion of
296 HSP101 from the *P. falciparum* PV does not sufficiently reduce PTEX activity to impact parasite
297 fitness under less taxing *in vitro* culture conditions.
298
299 **PV-localized function does not fully account for HSP101 contribution to parasite fitness**
300 To determine the amount of HSP101 needed to support parasite growth *in vitro*, we
301 combined knockER with the TetR-DOZI-aptamers system to generate a *P. falciparum* HSP101-
302 kER line that also allows for titration of HSP101 expression with aTc (Figure 6A). Like the original

303 HSP101-kER line, rapamycin-treated HSP101-kER$^{TetR-DOZI}$ parasites exhibited ER retention of
304 HSP101 without impacting parasite growth or export of representative PEXEL and PNEP proteins
305 (Figure 6B-D). However, HSP101 depletion following aTc washout resulted in a robust block in
306 protein export and parasite death (Figure 6D and S7A,B), consistent with previous HSP101
307 knockdown or inactivation studies (23-25). To determine the level of total HSP101 reduction
308 sufficient to impact growth, we grew synchronized parasites at a range of aTc concentrations
309 following DMSO or rapamycin treatment and measured mNG fluorescence via flow cytometry in
310 parallel with parasite growth (Figure 6E,F). Interestingly, rapamycin-treated parasites displayed a
311 small but reproducible increase in total HSP101, consistent with a reduction in HSP101 turnover
312 by endocytosis from the PV to the digestive vacuole following redistribution to the ER (Figure 6E).
313 More importantly, we determined that a ~70% reduction in total HSP101 levels was necessary to
314 impact parasite growth, showing that a relatively small amount of HSP101 is needed for survival
315 *in vitro* (Figure 6E,F, 5 nM aTc), consistent with redistribution of HSP101 by knockER not meeting
316 the threshold required to impact HSP101 PV function and parasite fitness.

317 If HSP101 functions exclusively in the PV, then knockER-mediated depletion of vacuolar
318 HSP101 levels should hypersensitize parasites to HSP101 knockdown. However, dose-response
319 to aTc was unaltered by rapamycin-treatment (Figure 6G), suggesting that the PV-localized
320 function of HSP101 does not fully account for its role in parasite fitness and implying an additional
321 important role in the ER. To further test this possibility, we generated an HSP101-knockER line
322 where mNG was replaced by a ligand-sensitive DHFR-based destabilization domain (DDD)
323 (Figure 6H) (24). In the absence of trimethoprim (TMP), the DDD blocks HSP101 interaction with
324 EXP2/PTEX150 but not cargo binding, specifically targeting function of the assembled PTEX
325 complex in the PV (24). In contrast to translational knockdown, HSP101-kER^{DDD} parasites were
326 hypersensitized to reduction of TMP levels following rapamycin-treatment, indicating a synergistic
327 effect when the reduction of HSP101 PV levels is combined with disruption of PTEX complex
328 formation (Figure 6I and S7C-E). Taken together, these results provide support for a distinct

329 HSP101 activity in the ER upstream of its PVM translocation function at the assembled PTEX
330 complex.
331
332 **Discussion**
333 Several genetic tools are now available for protein loss-of-function studies in *Plasmodium*
334 *spp.* (66), including knock-sideways for conditional sequestration of a target protein away from its
335 normal site of function (67, 68). While this system is not currently amenable to parasite proteins
336 that enter the secretory pathway, conditional control of secretory traffic has been achieved in *P.*
337 *falciparum* by ligand-mediated alteration of the N-terminal transit peptide that controls apicoplast
338 targeting, enabling redirection of plastid proteins into the default secretory pathway (69).
339 Additionally, conditional ER release systems have been developed in model eukaryotes based
340 on ER retrieval machinery (70). In contrast, knockER provides a simple, DiCre-mediated knock-
341 sideways strategy that exploits the ERD2/KDEL receptor (KDELR) system for conditional ER
342 retrieval, providing a generalizable approach for interrogating secreted proteins in genetically
343 tractable eukaryotes.
344 In this study, we demonstrate knockER simultaneously allows for trafficking and loss-of-
345 function studies. The ability to determine whether a protein traffics from the ER through the *cis*
346 Golgi is an important consideration for nuclear-encoded apicoplast proteins since Golgi-
347 dependent and -independent trafficking routes have been reported (32, 34, 71). While these
348 apicoplast trafficking studies were carried out with reporters and chimeras, knockER allows for
349 monitoring *cis* Golgi transit of endogenous proteins. The sensitivity of ClpB1 to KDEL-mediated
350 ER retrieval demonstrates a Golgi-dependent trafficking route to the apicoplast. Moreover, we
351 show for the first time that this AAA+ chaperone is essential for apicoplast maintenance. ClpB1 is
352 one of four Clp/HSP100 chaperones encoded by *Plasmodium spp*., three of which localize to the
353 parasite plastid while the fourth, HSP101 (previously known as ClpB2) localizes to the PV and
354 ER (44). The other apicoplast-targeted members of this quartet in include the nuclear-encoded

355 ClpC, which mediates regulated proteolysis together with the serine protease ClpP (72, 73), and
356 ClpM, now the only uncharacterized member of this group and one of the few proteins encoded
357 on the apicoplast genome. Similar to the well-studied function of its closest orthologs (74), ClpB1
358 likely acts as a disaggregase that, together with ClpC/P and ClpM, forms a critical proteostasis
359 system required to maintain and regulate the apicoplast proteome (75).

360 ER perturbations can trigger an integrated stress response leading to cell arrest or death
361 (76, 77). *Plasmodium* possesses one of the widely conserved ER stress sensors, the PERK-
362 eIF2α pathway which halts protein translation and flux through the secretory pathway (20, 78-81).
363 Importantly, conditional ER retrieval of proteins produced from their endogenous locus or by
364 heterologous expression was not generally toxic, enabling loss-of-function studies with knockER.
365 The single notable exception was EXP2, which rapidly killed parasites when retained in the ER
366 independent to loss of its PVM transport function, indicating knockER experiments should be
367 controlled for indirect effects. EXP2-KDEL toxicity was dependent on the amphipathic helix that
368 forms the membrane-spanning region in the oligomeric EXP2 pore (26), suggesting that
369 accumulation of EXP2 in the ER might trigger an unfolded protein response or lead to premature
370 pore formation in the early secretory pathway. More work is required to determine if this outcome
371 is specific to EXP2 or a general problem for unnatural ER-retrieval of membrane proteins. Indirect
372 fitness defects aside, retrieval of EXP2-KDEL demonstrates that its C-terminus enters the
373 secretory pathway lumen, consistent with a soluble EXP2 trafficking state that precedes
374 membrane integration at the PVM. Regardless of the basis for EXP2-kER toxicity, these
375 experiments highlight that knockER can also be used to investigate membrane topology. While
376 ER-resident type I membrane proteins utilize a different mechanism for retrieval as their C-termini
377 face the cytosol of the cell (82, 83), ERD2/KDELR can retrieve membrane proteins whose C-
378 termini face the lumen (84) and thus knockER should be able to distinguish the topology of single
379 and multi-pass transmembrane domain-containing proteins.

380 A unique feature of knockER is the ability to redistribute secreted proteins from their
381 terminal destination to the ER, providing a method to resolve potential HSP101 functions between
382 the PV and ER. We tagged both HSP101 and the translocon adaptor PTEX150 with knockER,
383 reasoning that ER retrieval of either protein would produce a lethal export defect but that
384 differential impacts on exported cargo trafficking might be exposed. Unexpectedly, ER retrieval of
385 HSP101 had no impact on *P. falciparum* growth or export of representative PEXEL and PNEP
386 proteins *in vitro*. Similar PV depletion of PTEX150 produced the anticipated lethal export block,
387 revealing that HSP101 PV levels are uniquely maintained in excess. As a AAA+ ATPase, HSP101
388 is the only enzyme in the PTEX core complex and its activity may exceed what is required to
389 support parasite fitness in the less demanding *in vitro* culture environment, as previously seen for
390 the aspartic protease Plasmepsin V that licenses proteins for export in the ER (85, 86). Indeed,
391 while critical to avoiding host defenses *in vivo*, most exported proteins are dispensable during *in*
392 *vitro* culture (12). Not surprisingly, ER retrieval of *P. berghei* HSP101 abolished parasite survival
393 in the mouse host, reinforcing the established PV function of HSP101 in effector translocation at
394 the PVM. In contrast, depletion of HSP101 PV levels in cultured *P. falciparum* likely impacts
395 translocon kinetics or export of specific proteins in ways that are not problematic for growth *in*
396 *vitro* and thus difficult to detect.

397 Importantly, redistribution of HSP101 from the PV to the ER hypersensitized parasites to
398 DDD-mediated HSP101 inactivation but not translational knockdown. While knockdown depletes
399 the entire HSP101 pool, HSP101-DDD acts post-translationally by disrupting complex formation
400 with EXP2/PTEX150 but not cargo recognition (24), specifically targeting HSP101 function in PVM
401 translocation. Together, these results indicate that the PV-localized function of HSP101 does not
402 fully account for its contribution to parasite fitness and provide the first functional genetic evidence
403 for an additional HSP101 function upstream of the PV, presumably in cargo recognition at the ER
404 and/or guiding export-destine proteins to PTEX, as recently proposed (23). Future work dissecting
405 the specific extra-vacuolar role(s) of HSP101 may resolve the long-standing question of how early

406 events in this pathway that mark proteins for export, such as PEXEL processing during ER entry,
407 are connected to cargo recognition and ultimate PVM translocation into the host cell at the
408 assembled PTEX complex.
409
410 **Materials and Methods**
411 **Parasite culture.** *P. falciparum* NF54$^{attB\text{-}DiCre}$ and derivatives were cultured in RPMI 1640 medium
412 supplemented with 27 mM sodium bicarbonate, 11 mM glucose, 0.37 mM hypoxanthine, 10 µg/ml
413 gentamicin and 0.5% Albumax I (Gibco). Parasites were maintained in deidentified, Institutional
414 Review Board-exempt RBCs obtained from the American National Red Cross. *P. berghei* ANKA
415 clone 2.34 and derivatives were maintained in Swiss Webster mice (Charles River). All
416 experiments involving rodents were reviewed and approved by the Iowa State University
417 Institutional Animal Care and Use Committee.
418
419 **Plasmids and genetic modification of *P. falciparum* and *P. berghei*.** All cloning was carried
420 out with NEBuilder HIFI DNA assembly (NEB). Primer sequences are given in Table S1. To
421 generate NF54$^{attB\text{-}DiCre}$ parasites, a DiCre expression cassette was inserted into the *pfs47* gene in
422 NF54^{attB} parasites (43) using a marker-free CRISPR/Cas9 editing strategy as described (28). Loss
423 of the endogenous *pfs47* locus was monitored with primers P1/2 and P3/4 and integration was
424 confirmed using primers P1/5 and P6/4. To confirm DiCre activity in this line, a loxP-flanked mNG
425 coding sequence with a 3xHA tag was PCR amplified using primers P19/20 and inserted between
426 AvrII and AflII in pLN-ENR-GFP cite (87), resulting in the plasmid JRB416. This plasmid was co-
427 transfected with pINT (87) into NF54$^{attB\text{-}DiCre}$ parasites and selection was applied with 2.5 µg/ml
428 blasticidin-S 24 hrs post-transfection.
429 To generate the kER fusion cassette, homology flanks targeting the 3' end of *exp2* were
430 amplified from pyPM2GT-EXP2-3xHA-GFP11 (54) using P21/22 and inserted between XhoI and
431 AvrII in pPM2GT-HSP101-3xFLAG (54). The loxPint sequence (29) was amplified with P23/24

432 and inserted immediately upstream of the 3xFLAG tag at AvrII in this vector. A partial loxPint
433 containing the loxP sequence and 3' portion of the intron followed by a 3xHA-KDEL tag was then
434 amplified with P25/26 and inserted into EagI, resulting in the plasmid JRB492. Finally, the mNG
435 coding sequencing was amplified from pyPM2GT-EXP2-mNG (88) with P27/28 and inserted into
436 AvrII in JRB492, resulting in plasmid JRB508.

437 To generate the SP-mNG-kER reporter, the *exp2* promoter and signal peptide were
438 amplified from parasite genomic DNA with P29/30 and the mNG-KER cassette was amplified from
439 JRB508 with P31/32 and these amplicons were assembled together in a second PCR reaction
440 with P29/32 and inserted into AscI/ApaI in pKD (42), resulting in the plasmid JRB543. For
441 expression of a second copy of EXP2-kER from the attB locus, the *exp2* promoter and full-length
442 gene were amplified from genomic DNA with P29/33 and inserted between AscI/BamHI in
443 JRB543, resulting in the plasmid JRB526. For expression of a second copy of EXP2-kER lacking
444 the amphipathic helix, a recoded portion of the *exp2* coding sequence beginning at codon 86
445 (after the amphipathic helix and immediately before the helical body domain) was amplified from
446 pEXP2^{apt} (54) and inserted at BamHI after the EXP2 signal peptide in JRB543, resulting in the
447 plasmid JRB544. These plasmids were each co-transfected with pINT and selected with 2.5 µg/ml
448 blasticidin-S as described above. To relieve translational repression by TetR-DOZI, parasite
449 cultures were supplemented with 500 nM aTc.

450 For generation of ClpB1-kER and RON6-kER lines, a Cas9 gRNA target was chosen just
451 downstream (*clpB1*, ATTTTTAGAAAAATATTATG) or just upstream (*ron6*,
452 TAATACATACAACGTACCAA) of the stop codon and the gRNA seed sequences were
453 synthesized as primers P34 and P35, respectively, and inserted into the AflII site of pAIO3 (40),
454 resulting in plasmids JRB143 and MAF22, respectively. To target the 3' end of *clpB1* or *ron6*, a 5'
455 homology flank (up to but not including the stop codon) was amplified from genomic DNA using
456 P36/37 or P38/39, incorporating synonymous shield mutations in the gRNA target sites. A 3'
457 homology flank was amplified using P40/41 or P42/43. The corresponding 5' and 3' flank

458 amplicons were assembled in a second PCR reaction using P40/37 and P42/39 and inserted
459 between XhoI/AvrII in JRB508, resulting in plasmids MAF20 and MAF27, respectively. These
460 plasmids were linearized with AflII and co-transfected with the corresponding Cas9/gRNA plasmid
461 into NF54$^{attB\text{-}DiCre}$. Selection was applied with 5 nM WR99120 24 hrs post-transfection and clonal
462 lines were isolated by limiting dilution after parasites returned from selection.

463 For generation of PTEX150-kER and HSP101-kER lines, flank assemblies targeting the
464 3' end of each gene were amplified using P44/45 from pyPM2GT-PTEX150-3xHA-GFP11 (54) or
465 P46/47 from pyPM2GT-HSP101-3xHA-GFP11 (54) and inserted between XhoI/AvrII in JRB508,
466 resulting in plasmids MAF16 and MAF17, respectively. These plasmids were linearized with AflII
467 and co-transfected with pAIO-PTEX150-CT-gRNA or pAIO-HSP101-CT-gRNA (54), selected with
468 5 nM WR99120 and cloned after parasites returned. For generation of the EXP2-kER line, plasmid
469 JRB492 (described above) was linearized and co-transfected with pUF-Cas9-EXP2-CT-gRNA
470 (54) and selected with 5 nM WR99120. For generation of HSP101-kER$^{TetR\text{-}DOZI}$ lines, flank
471 assembles were amplified using P48/49 and inserted between AscI/BamHI in JRB526 (described
472 above), resulting in plasmid MAF41. This plasmid was linearized with AflII and co-transfected with
473 pAIO-HSP101-CT-gRNA, selected with 2.5 µg/ml blasticidin-S and 500 nM aTc, and cloned after
474 parasites returned. For generation of HSP101-kER^{DDD} lines, the DDD was amplified from plasmid
475 pPM2GT-HSP101-3xFlag-DDD (54) using P70/71 and inserted between AvrII/BsrGI in MAF17,
476 replacing the mNG and resulting in plasmid MAF43. This plasmid was linearized with AflII and co-
477 transfected with pAIO-HSP101-CT-gRNA. Selection was applied with 10 µM TMP 24 hrs post-
478 transfection.

479 For expression of a second copy of PTEX150-kER from the *attB* locus, the *ptex150*
480 promoter and full-length gene were amplified from genomic DNA with P50/51 and the mNG-KER
481 cassette was amplified from JRB508 with P52/53. These amplicons were assembled together in
482 a second PCR reaction using P50/53 and inserted between ApaI/AflII in pLN-ENR-GFP (87),

483 resulting in the plasmid MAF39. This plasmid was co-transfected with pINT, selected with 2.5
484 µg/ml blasticidin-S and parasites were cloned after returning.

485 To generate the line bearing endogenous EXP2-mRuby and HSP101-mNG tags, the
486 plasmid pbEXP2-mRuby3 (89) was first linearized with AflII and co-transfected with pUF-Cas9-
487 EXP2-CT-gRNA (54) into NF54$^{attB\text{-}DiCre}$. Selection was applied with 2.5 µg/ml blasticidin-S. Next,
488 the mNG coding sequence was amplified using P54/55 and inserted between AvrII/EagI in
489 pPM2GT-HSP101-3xFLAG (54) to replace the FLAG tag with mNG, resulting in the plasmid
490 JRB325. This plasmid was linearized with AflII and co-transfected with pAIO-HSP101-CT-gRNA
491 (89) into the NF54$^{attB\text{-}DiCre}$::EXP2-mRuby parasites. Selection was applied with 5nM WR99120
492 resulting in the line NF54$^{attB\text{-}DiCre}$::EXP2-mRuby+HSP101-mNG.

493 For generation of PTEX150-kER and HSP101-kER lines in *P. berghei*, the plasmid pBAT
494 (90) was digested with MluI/XhoI and the primer P56 was used as an insert to remove the
495 intervening AvrII, SnaBI and XhoI sites from the MCS. Next, the mRuby3 coding sequence fused
496 to the PbEXP2 signal peptide was amplified with P57/58 and inserted between SwaI/BamHI,
497 replacing the GFP. The mNG-kER tagging sequence was amplified from plasmid JRB508 using
498 P59/60 and inserted between SacII/SphI, replacing the mCherry-3xMYC. Finally, 5' flanks to tag
499 *P. berghei hsp101* or *ptex150* with mNG-kER were amplified from *P. berghei* genomic DNA using
500 P61/62 or P63/64, respectively, and 3' flanks were amplified using P65/66 or P67/68, respectively.
501 The corresponding 5' and 3' flank amplicons were assembled with an intervening AflII site in a
502 second PCR reaction using P65/62 or P67/64, respectively, and inserted at SacII, resulting in
503 plasmids pPbHSP101-kER and pPbPTEX150-kER. The plasmids were linearized at AflII and
504 transfected as described (91) into the marker-free HP DiCre line (92). Transfected parasites were
505 reinjected into naïve mice and selection was applied with 0.07 mg/ml pyrimethamine in drinking
506 water provided *ad libitum* 24 hours later. After returning from selection, transfected populations
507 were cloned by limiting dilution IV injection into naïve mice to generate isogenic populations
508 designated PbHSP101-kER and PbPTEX150-kER.

509

510 ***P. falciparum* growth assays**. Growth assays were performed as described previously (93).
511 Briefly, parasites were treated with either DMSO or 10 nM rapamycin for 3 hrs and washed 1X.
512 Then, parasites were seeded between 0.2-1% parasitemia in triplicate and monitored every 48
513 hrs by flow cytometry on an Attune NxT (ThermoFisher) by nucleic acid staining with PBS
514 containing 0.8 µg/ml acridine orange. For IPP rescue experiments, ClpB1-kER cultures were
515 supplemented with 200 µM IPP. For kER fusions expressed from the *attB* locus, cultures were
516 supplemented with 1 µM aTc 24 hrs prior to rapamycin treatment to relieve TetR-DOZI-aptamer
517 translational repression. For HSP101-kER$^{TetR\text{-}DOZI}$ parasites, aTc was removed by washing
518 parasites 7X with 13 mL of media. 500 nM aTc was then supplemented back to control parasites.
519 As required, parasites were sub-cultured to avoid high parasite density, and relative parasitemia
520 at each time point was back-calculated based on actual parasitemia multiplied by the relevant
521 dilution factors. Data were displayed using Prism 9 (GraphPad Software).

522 For EC_{50} shift assays of HSP101-kER$^{TetR\text{-}DOZI}$ and HSP101-kER^{DDD}, asynchronous
523 parasites were treated with DMSO or rapamycin before removal of aTc or TMP. After agonist
524 washout as described above, parasites were seeded in triplicate at 0.5% parasitemia with 2-fold
525 dilutions starting from 500 nM aTc or 250 nM TMP and parasite growth was monitored after 72
526 hrs.

527

528 ***P. berghei* kER experiments.** Parasite-infected blood was collected by cardiac puncture when
529 parasitemia reached 3-4% and cultured in RPMI supplemented with 20% FBS. Cultures were
530 treated with 10 nM rapamycin or a DMSO vehicle control for 3 hours followed by a media change.
531 After 18 hours of additional culture, parasites were harvested for diagnostic PCR, live
532 fluorescence microscopy and Western blot. Equal numbers of DMSO or rapamycin-treated
533 infected RBCs (~10,000 parasites per injection) were IV injected into naïve mice and parasitemia
534 was monitored by giemsa-stained blood smear every two days.

535

536 **Microscopy.** For live microscopy, *P. falciparum* parasites were treated with either DMSO or 10
537 nM rapamycin and viewed 24-48 hrs later. Hoechst (33342, Invitrogen; 1:10,000) was used to
538 visualize the nucleus by incubating with parasites 2-5 min prior to visualization. ER-Tracker Red
539 (Invitrogen; 1:1000) was used to visualize the ER by incubating with parasites 30 min at 37°C
540 prior to visualization. For constructs expressed from the *attB* locus under TetR-DOZI-aptamers
541 control, parasites were grown in 1 μM aTc for 24 hrs prior to incubation with DMSO or rapamycin
542 to allow expression. For *P. berghei*, parasites were isolated via cardiac puncture, treated with
543 DMSO or rapamycin for 3 hrs and allowed to develop overnight in culture before visualization. For
544 quantification of fluorescence signal, MFI was calculated using the measured Integrated Density
545 value from Fiji (94). The internal MFI was calculated using an ROI within the parasite PV and
546 subtracting that from the whole parasite MFI using an ROI outside the PV boundary. The percent
547 internal fluorescence was then calculated by dividing the internal MFI by the whole parasite MFI.
548 For protease protection assays on live cells, parasites were treated with 0.03% saponin
549 (Sigma) in 1X PBS for 15 min at 4°C. Purified parasites where then washed once with 5 mL of 1X
550 PBS and once with 5 mL of digestion buffer (50 mM Tris pH 7.5, 150 mM NaCl, 1 mM $CaCl_2$) (23).
551 Parasite samples where then split into two identical tubes, one of which was treated with 20 μg/mL
552 of Proteinase K (740506.75, Macherey-Nagel), and incubated at 37°C for 15 min. Proteinase K
553 was removed and samples resuspended with digestion buffer plus protease inhibitor cocktail (Halt
554 78429, Thermo Scientific) before visualization.
555 For IFAs of the EXP2- and ClpB1-kER lines, parasites were treated with either DMSO or
556 10 nM rapamycin and fixed 24 hrs or 144 hrs later as described previously (93). For HSP101-
557 $kER^{TetR\text{-}DOZI}$ lines, parasites were synchronized with 5% sorbitol, treated with either DMSO or 10
558 nM rapamycin, grown with or without 500 nM aTc, and fixed 48 hrs later. Briefly, parasites were
559 fixed with Fixative Solution (4% paraformaldehyde, 0.0075% glutaraldehyde in PBS) for 25 min
560 at room temperature in the dark. Parasites were then permeabilized with 0.1% Triton in PBS for

561 10 minutes at room temperature while rocking. Parasites were washed 1X with PBS and then
562 blocked with 3% BSA in PBS for 1hr at room temperature. Primary antibody was applied in 3%
563 BSA solution for 1 hr at room temperature, washed 2X with PBS, followed by secondary antibody
564 incubation for 1 hr at room temperature. After 2X washes with PBS, parasites were adhered onto
565 Poly-L-lysine covered coverslips and then mounted onto slides. For parasites probed with SBP1,
566 parasites were acetone fixed as in (40). Briefly, thin smears were immersed in 100% acetone for
567 2 min. Smears were washed 1X with PBS and then blocked with 3% BSA in PBS for 1 hr at room
568 temperature. Primary antibody was applied in 3% BSA solution for 1 hr at room temperature,
569 washed 2X with PBS, followed by secondary antibody incubation for 1 hr at room temperature.
570 After 2X washes with PBS, slides were mounted with DAPI, covered with a coverslip and sealed.
571 The antibodies used for IFA were: mouse anti-HA antibody (clone 16B12; BioLegend, 1:200 IFA),
572 rabbit polyclonal anti-HA SG77 (ThermoFisher; 1:500 IFA), rabbit anti-PfGRP78 (BiP) (MRA-
573 1246; BEI Resources, NIAID, NIH 1:100), mouse monoclonal anti-FLAG clone M2 (Sigma-Aldrich,
574 1:200 IFA), rabbit monoclonal anti-Flag 8H8L17 (ThermoFisher; 1:500 IFA), mouse anti-HRP2
575 clone 2G12 (1:500 IFA) (95), rabbit polyclonal anti-SBP1 (BR28, 1:500 IFA) (96), mouse
576 monoclonal anti-EXP2 clone 7.7 (1:500 WB) (97), and rabbit polyclonal anti-ACP1 (1:500 IFA)
577 (38, 98). Secondary antibodies used were anti-mouse antibody conjugated to Alexa Fluor 488 or
578 546 and anti-rabbit antibody conjugated to Alexa Fluor 488, (Life Technologies, 1:1000). Parasites
579 were mounted with ProLong diamond with 4',6'-diamidino-2-phenylindole (DAPI) (P36931;
580 Invitrogen) and imaged on an Axio Observer 7 equipped with an Axiocam 702 mono camera and
581 Zen 2.6 Pro software (Zeiss) using the same exposure times for all images across sample groups
582 and experimental replicates. Image processing, analysis, and display were performed using Zeiss
583 Blue software and Adobe Photoshop. Equivalent adjustments to brightness and contrast were
584 made within sample groups for display purposes.
585

586 **Quantification of protein knockdown.** To evaluate the level of HSP101 protein knockdown,
587 HSP101-kER$^{TetR-DOZI}$ parasites were synchronized via magnet purification and treated with DMSO
588 or rapamycin before removal of aTc. After aTc removal, parasites were seeded at ~1%
589 parasitemia with different dilutions of aTc and allowed to grow for 48 hrs. Using an Attune NxT
590 flow cytometer (ThermoFisher), infected RBCs were gated using Hoechst (34580, Invitrogen) and
591 mNG fluorescence of infected RBCs was concurrently measured. The same procedure was
592 applied for saponin-released parasites after protease treatment as described above.
593
594 **Western blotting.** Western blotting was performed as described previously (40, 54). Briefly,
595 parasite-infected RBCs were selectively permeabilized by treatment with ice-cold 0.03% saponin
596 in PBS for 15 min followed by lysis with RIPA and centrifugation to remove hemozoin. For
597 constructs expressed from the *attB* locus under control of TetR-DOZI-aptamers, parasites were
598 grown in 500 nM aTc for 24 hrs prior to incubation with DMSO or rapamycin to allow for
599 expression. For the HSP101-kER$^{TetR-DOZI}$ lines, parasites were treated with DMSO or rapamycin
600 before removal of aTc. After aTc removal, parasites were seeded at ~1% parasitemia with
601 different dilutions of aTc and allowed to grow for 48 hrs before processing. The antibodies used
602 in this study were mouse anti-HA antibody (clone 16B12; BioLegend, 1:500), rabbit polyclonal
603 anti-HA SG77 (ThermoFisher; 1:500), mouse anti-FLAG (Clone M2; Sigma-Aldrich, 1:500), rabbit
604 polyclonal anti-*Plasmodium* Aldolase ab207494 (Abcam; 1:500) and mouse anti-EXP2 (Clone
605 7.7; 1:500). The secondary antibodies used were IRDye 680CW goat anti-rabbit IgG and IRDye
606 800CW goat anti-mouse IgG (Li-COR Biosciences, 1:20,000). Western blot images were acquired
607 using an Odyssey Clx infrared imaging system and processed with Image Studio software (Li-
608 COR Biosciences). Full length versions of cropped blots can be seen in Figure S8.
609
610 **Acknowledgements**

611 This work was supported by NIH grant HL133453 to JRB. The funders had no role in study design,
612 data collection and interpretation, or the decision to submit the work for publication. We thank J.
613 McBride, D. Cavanaugh and EMRR for the EXP2 antibody and A. Waters for the HP DiCre *P.*
614 *berghei* parasites.

615

616 **Author contributions**

617 M.A.F. and J.R.B designed research; M.A.F., T.H., L.J.C. and J.R.B performed research; M.A.F.
618 and J.R.B analyzed data; M.A.F. and J.R.B. wrote the paper.

619 **References**

620 1. G. G. van Dooren, B. Striepen, The algal past and parasite present of the apicoplast.
621 *Annu Rev Microbiol* **67**, 271-289 (2013).

622 2. O. A. Akuh, R. Elahi, S. T. Prigge, F. Seeber, The ferredoxin redox system - an essential
623 electron distributing hub in the apicoplast of Apicomplexa. *Trends Parasitol* **38**, 868-881
624 (2022).

625 3. M. M. Cova, M. H. Lamarque, M. Lebrun, How Apicomplexa Parasites Secrete and Build
626 Their Invasion Machinery. *Annu Rev Microbiol* **76**, 619-640 (2022).

627 4. J. M. Matz, J. R. Beck, M. J. Blackman, The parasitophorous vacuole of the blood-stage
628 malaria parasite. *Nat Rev Microbiol* **18**, 379-391 (2020).

629 5. M. Garten, J. R. Beck, Structured to conquer: transport across the Plasmodium
630 parasitophorous vacuole. *Curr Opin Microbiol* **63**, 181-188 (2021).

631 6. T. F. de Koning-Ward, M. W. Dixon, L. Tilley, P. R. Gilson, Plasmodium species: master
632 renovators of their host cells. *Nat Rev Microbiol* **14**, 494-507 (2016).

633 7. J. R. Beck, C. M. Ho, Transport mechanisms at the malaria parasite-host cell interface.
634 *PLoS Pathog* **17**, e1009394 (2021).

635 8. T. J. Sargeant *et al.*, Lineage-specific expansion of proteins exported to erythrocytes in
636 malaria parasites. *Genome Biol* **7**, R12 (2006).

637 9. J. A. Boddey *et al.*, Role of plasmepsin V in export of diverse protein families from the
638 Plasmodium falciparum exportome. *Traffic* **14**, 532-550 (2013).

639 10. C. van Ooij *et al.*, The malaria secretome: from algorithms to essential function in blood
640 stage infection. *PLoS Pathog* **4**, e1000084 (2008).

641 11. J. Schulze *et al.*, The Plasmodium falciparum exportome contains non-canonical
642 PEXEL/HT proteins. *Mol Microbiol* **97**, 301-314 (2015).

643 12. T. K. Jonsdottir, M. Gabriela, B. S. Crabb, F. d. K.-W. T, P. R. Gilson, Defining the
644 Essential Exportome of the Malaria Parasite. *Trends Parasitol* **37**, 664-675 (2021).

645 13. A. Florentin, D. W. Cobb, H. M. Kudyba, V. Muralidharan, Directing traffic: Chaperone-
646 mediated protein transport in malaria parasites. *Cell Microbiol* **22**, e13215 (2020).

647 14. S. Munro, H. R. Pelham, A C-terminal signal prevents secretion of luminal ER proteins.
648 *Cell* **48**, 899-907 (1987).

649 15. P. Brauer *et al.*, Structural basis for pH-dependent retrieval of ER proteins from the Golgi
650 by the KDEL receptor. *Science* **363**, 1103-1107 (2019).

651 16. A. Gerondopoulos *et al.*, A signal capture and proofreading mechanism for the KDEL-
652 receptor explains selectivity and dynamic range in ER retrieval. *Elife* **10** (2021).

653 17. H. G. Elmendorf, K. Haldar, Identification and localization of ERD2 in the malaria
654 parasite Plasmodium falciparum: separation from sites of sphingomyelin synthesis and
655 implications for organization of the Golgi. *EMBO J* **12**, 4763-4773 (1993).

656 18. N. La Greca, A. R. Hibbs, C. Riffkin, M. Foley, L. Tilley, Identification of an endoplasmic
657 reticulum-resident calcium-binding protein with multiple EF-hand motifs in asexual
658 stages of Plasmodium falciparum. *Mol Biochem Parasitol* **89**, 283-293 (1997).

659 19. S. Kulzer, N. Gehde, J. M. Przyborski, Return to sender: use of Plasmodium ER retrieval
660 sequences to study protein transport in the infected erythrocyte and predict putative ER
661 protein families. *Parasitol Res* **104**, 1535-1541 (2009).

662 20. H. M. Kudyba *et al.*, The endoplasmic reticulum chaperone PfGRP170 is essential for
663 asexual development and is linked to stress response in malaria parasites. *Cell Microbiol*
664 **21**, e13042 (2019).

665 21. M. A. Fierro *et al.*, An ER CREC family protein regulates the egress proteolytic cascade
666 in malaria parasites. *bioRxiv*, 457481 (2019).

667 22. D. W. Cobb *et al.*, A redox-active crosslinker reveals an essential and inhibitable
668 oxidative folding network in the endoplasmic reticulum of malaria parasites. *PLoS*
669 *Pathog* **17**, e1009293 (2021).

670 23. M. Gabriela *et al.*, A revised mechanism for how Plasmodium falciparum recruits and
671 exports proteins into its erythrocytic host cell. *PLoS Pathog* **18**, e1009977 (2022).

672 24. J. R. Beck, V. Muralidharan, A. Oksman, D. E. Goldberg, PTEX component HSP101
673 mediates export of diverse malaria effectors into host erythrocytes. *Nature* **511**, 592-595
674 (2014).

675 25. B. Elsworth *et al.*, PTEX is an essential nexus for protein export in malaria parasites.
676 *Nature* **511**, 587-591 (2014).

677 26. C. M. Ho *et al.*, Malaria parasite translocon structure and mechanism of effector export.
678 *Nature* **561**, 70-75 (2018).

679 27. C. R. Collins *et al.*, Robust inducible Cre recombinase activity in the human malaria
680 parasite Plasmodium falciparum enables efficient gene deletion within a single asexual
681 erythrocytic growth cycle. *Mol Microbiol* **88**, 687-701 (2013).

682 28. E. Knuepfer, M. Napiorkowska, C. van Ooij, A. A. Holder, Generating conditional gene
683 knockouts in Plasmodium - a toolkit to produce stable DiCre recombinase-expressing
684 parasite lines using CRISPR/Cas9. *Sci Rep* **7**, 3881 (2017).

685 29. M. L. Jones *et al.*, A versatile strategy for rapid conditional genome engineering using
686 loxP sites in a small synthetic intron in Plasmodium falciparum. *Sci Rep* **6**, 21800 (2016).

687 30. J. M. Przyborski *et al.*, Trafficking of STEVOR to the Maurer's clefts in Plasmodium
688 falciparum-infected erythrocytes. *EMBO J* **24**, 2306-2317 (2005).

689 31. G. G. van Dooren *et al.*, Development of the endoplasmic reticulum, mitochondrion and
690 apicoplast during the asexual life cycle of Plasmodium falciparum. *Mol Microbiol* **57**, 405-
691 419 (2005).

692 32. C. J. Tonkin, N. S. Struck, K. A. Mullin, L. M. Stimmler, G. I. McFadden, Evidence for
693 Golgi-independent transport from the early secretory pathway to the plastid in malaria
694 parasites. *Mol Microbiol* **61**, 614-630 (2006).

695 33. M. C. Lee, P. A. Moura, E. A. Miller, D. A. Fidock, Plasmodium falciparum Sec24 marks
696 transitional ER that exports a model cargo via a diacidic motif. *Mol Microbiol* **68**, 1535-
697 1546 (2008).

698 34. S. R. Heiny, S. Pautz, M. Recker, J. M. Przyborski, Protein Traffic to the Plasmodium
699 falciparum apicoplast: evidence for a sorting branch point at the Golgi. *Traffic* **15**, 1290-
700 1304 (2014).

701 35. J. M. Matz *et al.*, The Plasmodium berghei translocon of exported proteins reveals
702 spatiotemporal dynamics of tubular extensions. *Sci Rep* **5**, 12532 (2015).

703 36. M. J. Boucher *et al.*, Integrative proteomics and bioinformatic prediction enable a high-
704 confidence apicoplast proteome in malaria parasites. *PLoS Biol* **16**, e2005895 (2018).

705 37. J. Birnbaum *et al.*, A Kelch13-defined endocytosis pathway mediates artemisinin
706 resistance in malaria parasites. *Science* **367**, 51-59 (2020).

707 38. R. F. Waller, M. B. Reed, A. F. Cowman, G. I. McFadden, Protein trafficking to the
708 plastid of Plasmodium falciparum is via the secretory pathway. *EMBO J* **19**, 1794-1802
709 (2000).

710 39. A. Adisa *et al.*, The signal sequence of exported protein-1 directs the green fluorescent
711 protein to the parasitophorous vacuole of transfected malaria parasites. *J Biol Chem*
712 **278**, 6532-6542 (2003).

713 40. T. Nessel *et al.*, EXP1 is required for organisation of EXP2 in the intraerythrocytic
714 malaria parasite vacuole. *Cell Microbiol* **22**, e13168 (2020).

715 41. S. M. Ganesan, A. Falla, S. J. Goldfless, A. S. Nasamu, J. C. Niles, Synthetic RNA-
716 protein modules integrated with native translation mechanisms to control gene
717 expression in malaria parasites. *Nat Commun* **7**, 10727 (2016).

718 42. K. Rajaram, H. B. Liu, S. T. Prigge, Redesigned TetR-Aptamer System To Control Gene
719 Expression in Plasmodium falciparum. *mSphere* **5** (2020).

720 43. S. H. Adjalley *et al.*, Quantitative assessment of Plasmodium falciparum sexual
721 development reveals potent transmission-blocking activity by methylene blue. *Proc Natl*
722 *Acad Sci U S A* **108**, E1214-1223 (2011).

723 44. M. El Bakkouri *et al.*, The Clp chaperones and proteases of the human malaria parasite
724 Plasmodium falciparum. *J Mol Biol* **404**, 456-477 (2010).

725 45. E. Yeh, J. L. DeRisi, Chemical rescue of malaria parasites lacking an apicoplast defines
726 organelle function in blood-stage Plasmodium falciparum. *PLoS Biol* **9**, e1001138
727 (2011).

728 46. G. G. van Dooren, V. Su, M. C. D'Ombrain, G. I. McFadden, Processing of an apicoplast
729 leader sequence in Plasmodium falciparum and the identification of a putative leader
730 cleavage enzyme. *J Biol Chem* **277**, 23612-23619 (2002).

731 47. M. Zhang *et al.*, Uncovering the essential genes of the human malaria parasite
732 Plasmodium falciparum by saturation mutagenesis. *Science* **360** (2018).

733 48. E. Bushell *et al.*, Functional Profiling of a Plasmodium Genome Reveals an Abundance
734 of Essential Genes. *Cell* **170**, 260-272 e268 (2017).

735 49. M. E. Fichera, D. S. Roos, A plastid organelle as a drug target in apicomplexan
736 parasites. *Nature* **390**, 407-409 (1997).

737 50. E. L. Dahl, P. J. Rosenthal, Multiple antibiotics exert delayed effects against the
738 Plasmodium falciparum apicoplast. *Antimicrob Agents Chemother* **51**, 3485-3490 (2007).

739 51. N. I. Proellocks *et al.*, Characterisation of PfRON6, a Plasmodium falciparum rhoptry
740 neck protein with a novel cysteine-rich domain. *Int J Parasitol* **39**, 683-692 (2009).

741 52. S. A. Desai, D. J. Krogstad, E. W. McCleskey, A nutrient-permeable channel on the
742 intraerythrocytic malaria parasite. *Nature* **362**, 643-646 (1993).

743 53. S. A. Desai, R. L. Rosenberg, Pore size of the malaria parasite's nutrient channel. *Proc*
744 *Natl Acad Sci U S A* **94**, 2045-2049 (1997).

745 54. M. Garten *et al.*, EXP2 is a nutrient-permeable channel in the vacuolar membrane of
746 Plasmodium and is essential for protein export via PTEX. *Nat Microbiol* **3**, 1090-1098
747 (2018).

748 55. D. A. Gold *et al.*, The Toxoplasma Dense Granule Proteins GRA17 and GRA23 Mediate
749 the Movement of Small Molecules between the Host and the Parasitophorous Vacuole.
750 *Cell Host Microbe* **17**, 642-652 (2015).

751 56. P. R. Sanders *et al.*, The N-terminus of EXP2 forms the membrane-associated pore of
752 the protein exporting translocon PTEX in Plasmodium falciparum. *J Biochem* **165**, 239-
753 248 (2019).

754 57. K. Hakamada, H. Watanabe, R. Kawano, K. Noguchi, M. Yohda, Expression and
755 characterization of the Plasmodium translocon of the exported proteins component
756 EXP2. *Biochem Biophys Res Commun* **482**, 700-705 (2017).

757 58. M. Dal Peraro, F. G. van der Goot, Pore-forming toxins: ancient, but never really out of
758 fashion. *Nat Rev Microbiol* **14**, 77-92 (2016).

759 59. S. C. Charnaud, R. Kumarasingha, H. E. Bullen, B. S. Crabb, P. R. Gilson, Knockdown
760 of the translocon protein EXP2 in Plasmodium falciparum reduces growth and protein
761 export. *PLoS One* **13**, e0204785 (2018).

762 60. T. F. de Koning-Ward *et al.*, A newly discovered protein export machine in malaria
763 parasites. *Nature* **459**, 945-949 (2009).

764 61. S. C. Charnaud *et al.*, Spatial organization of protein export in malaria parasite blood
765 stages. *Traffic* **19**, 605-623 (2018).

766 62. S. Nair *et al.*, Nutrient Limitation Magnifies Fitness Costs of Antimalarial Drug
767 Resistance Mutations. *Antimicrob Agents Chemother* **66**, e0152921 (2022).

768 63. A. Gupta *et al.*, Complex nutrient channel phenotypes despite Mendelian inheritance in a
769 Plasmodium falciparum genetic cross. *PLoS Pathog* **16**, e1008363 (2020).

770 64. J. M. Matz *et al.*, In Vivo Function of PTEX88 in Malaria Parasite Sequestration and
771 Virulence. *Eukaryot Cell* **14**, 528-534 (2015).

772 65. S. A. Chisholm *et al.*, Contrasting Inducible Knockdown of the Auxiliary PTEX
773 Component PTEX88 in P. falciparum and P. berghei Unmasks a Role in Parasite
774 Virulence. *PLoS One* **11**, e0149296 (2016).

775 66. H. M. Kudyba, D. W. Cobb, J. Vega-Rodriguez, V. Muralidharan, Some conditions apply:
776 Systems for studying Plasmodium falciparum protein function. *PLoS Pathog* **17**,
777 e1009442 (2021).

778 67. J. Birnbaum *et al.*, A genetic system to study Plasmodium falciparum protein function.
779 *Nat Methods* **14**, 450-456 (2017).

780 68. K. R. Hughes, A. P. Waters, Rapid inducible protein displacement in. *Wellcome Open*
781 *Res* **2**, 18 (2017).

782 69. A. D. Roberts, S. C. Nair, A. J. Guerra, S. T. Prigge, Development of a conditional
783 localization approach to control apicoplast protein trafficking in malaria parasites. *Traffic*
784 **20**, 571-582 (2019).

785 70. A. Praznik *et al.*, Regulation of protein secretion through chemical regulation of
786 endoplasmic reticulum retention signal cleavage. *Nat Commun* **13**, 1323 (2022).

787 71. A. Prasad, P. Mastud, S. Patankar, Dually localised proteins found in both the apicoplast
788 and mitochondrion utilize the Golgi-dependent pathway for apicoplast targeting in
789 Toxoplasma gondii. *Biol Cell* **113**, 58-78 (2021).

790 72. A. Florentin *et al.*, PfClpC Is an Essential Clp Chaperone Required for Plastid Integrity
791 and Clp Protease Stability in Plasmodium falciparum. *Cell Rep* **21**, 1746-1756 (2017).

792 73. A. Florentin, D. R. Stephens, C. F. Brooks, R. P. Baptista, V. Muralidharan, Plastid
793 biogenesis in malaria parasites requires the interactions and catalytic activity of the Clp
794 proteolytic system. *Proc Natl Acad Sci U S A* **117**, 13719-13729 (2020).

795 74. A. Mogk, B. Bukau, H. H. Kampinga, Cellular Handling of Protein Aggregates by
796 Disaggregation Machines. *Mol Cell* **69**, 214-226 (2018).

797 75. I. Bouchnak, K. J. van Wijk, Structure, function, and substrates of Clp AAA+ protease
798 systems in cyanobacteria, plastids, and apicoplasts: A comparative analysis. *J Biol*
799 *Chem* **296**, 100338 (2021).

800 76. K. Pakos-Zebrucka *et al.*, The integrated stress response. *EMBO Rep* **17**, 1374-1395
801 (2016).

802 77. M. Costa-Mattioli, P. Walter, The integrated stress response: From mechanism to
803 disease. *Science* **368** (2020).

804 78. S. Chaubey, M. Grover, U. Tatu, Endoplasmic reticulum stress triggers
805 gametocytogenesis in the malaria parasite. *J Biol Chem* **289**, 16662-16674 (2014).

806 79. M. B. Harbut *et al.*, Targeting the ERAD pathway via inhibition of signal peptide
807 peptidase for antiparasitic therapeutic design. *Proc Natl Acad Sci U S A* **109**, 21486-
808 21491 (2012).

809 80. M. Zhang *et al.*, PK4, a eukaryotic initiation factor 2alpha(eIF2alpha) kinase, is essential
810 for the development of the erythrocytic cycle of Plasmodium. *Proc Natl Acad Sci U S A*
811 **109**, 3956-3961 (2012).

812 81. M. Zhang *et al.*, Inhibiting the Plasmodium eIF2alpha Kinase PK4 Prevents Artemisinin-
813 Induced Latency. *Cell Host Microbe* **22**, 766-776 e764 (2017).

814 82. E. C. Gaynor, S. te Heesen, T. R. Graham, M. Aebi, S. D. Emr, Signal-mediated retrieval
815 of a membrane protein from the Golgi to the ER in yeast. *J Cell Biol* **127**, 653-665
816 (1994).

817 83. M. Stornaiuolo *et al.*, KDEL and KKXX retrieval signals appended to the same reporter
818 protein determine different trafficking between endoplasmic reticulum, intermediate
819 compartment, and Golgi complex. *Mol Biol Cell* **14**, 889-902 (2003).

820 84. B. L. Tang, S. H. Wong, S. H. Low, W. J. Hong, Retention of a Type-Ii Surface-
821 Membrane Protein in the Endoplasmic-Reticulum by the Lys-Asp-Glu-Leu Sequence.
822 *Journal of Biological Chemistry* **267**, 7072-7076 (1992).

823 85. B. E. Sleebs *et al.*, Inhibition of Plasmepsin V activity demonstrates its essential role in
824 protein export, PfEMP1 display, and survival of malaria parasites. *PLoS Biol* **12**,
825 e1001897 (2014).

826 86. A. J. Polino, A. S. Nasamu, J. C. Niles, D. E. Goldberg, Assessment of Biological Role
827 and Insight into Druggability of the Plasmodium falciparum Protease Plasmepsin V. *ACS*
828 *Infect Dis* **6**, 738-746 (2020).

829 87. S. H. Adjalley, M. C. S. Lee, D. A. Fidock, "A Method for Rapid Genetic Integration into
830 Plasmodium falciparum Utilizing Mycobacteriophage Bxb1 Integrase". (Humana Press,
831 2010), pp. 87-100.

832 88. S. Glushakova *et al.*, Exploitation of a newly-identified entry pathway into the malaria
833 parasite-infected erythrocyte to inhibit parasite egress. *Sci Rep* **7**, 12250 (2017).

834 89. A. I. Ahiya, S. Bhatnagar, J. M. Morrisey, J. R. Beck, A. B. Vaidya, Dramatic
835 Consequences of Reducing Erythrocyte Membrane Cholesterol on Plasmodium
836 falciparum. *Microbiol Spectr* **10**, e0015822 (2022).

837 90. T. W. Kooij, M. M. Rauch, K. Matuschewski, Expansion of experimental genetics
838 approaches for Plasmodium berghei with versatile transfection vectors. *Mol Biochem*
839 *Parasitol* **185**, 19-26 (2012).

840 91. C. J. Janse, J. Ramesar, A. P. Waters, High-efficiency transfection and drug selection of
841 genetically transformed blood stages of the rodent malaria parasite Plasmodium berghei.
842 *Nat Protoc* **1**, 346-356 (2006).

843 92. R. S. Kent *et al.*, Inducible developmental reprogramming redefines commitment to
844 sexual development in the malaria parasite Plasmodium berghei. *Nat Microbiol* **3**, 1206-
845 1213 (2018).

846 93. M. A. Fierro *et al.*, An Endoplasmic Reticulum CREC Family Protein Regulates the
847 Egress Proteolytic Cascade in Malaria Parasites. *mBio* **11** (2020).

848 94. J. Schindelin *et al.*, Fiji: an open-source platform for biological-image analysis. *Nat*
849 *Methods* **9**, 676-682 (2012).

850 95. E. P. Rock *et al.*, Comparative analysis of the Plasmodium falciparum histidine-rich
851 proteins HRP-I, HRP-II and HRP-III in malaria parasites of diverse origin. *Parasitology*
852 **95 (Pt 2)**, 209-227 (1987).

853 96. T. Blisnick *et al.*, Pfsbp1, a Maurer's cleft Plasmodium falciparum protein, is associated
854 with the erythrocyte skeleton. *Mol Biochem Parasitol* **111**, 107-121 (2000).

855 97. R. Hall *et al.*, Antigens of the Erythrocytic Stages of the Human Malaria Parasite
856 Plasmodium-Falciparum Detected by Monoclonal-Antibodies. *Molecular and*
857 *Biochemical Parasitology* **7**, 247-265 (1983).

858 98. M. Ponpuak *et al.*, A role for falcilysin in transit peptide degradation in the Plasmodium
859 falciparum apicoplast. *Mol Microbiol* **63**, 314-334 (2007).

860 99. K. Matthews *et al.*, The Plasmodium translocon of exported proteins (PTEX) component
861 thioredoxin-2 is important for maintaining normal blood-stage growth. *Mol Microbiol* **89**,
862 1167-1186 (2013).

863

864

865 **Figures**

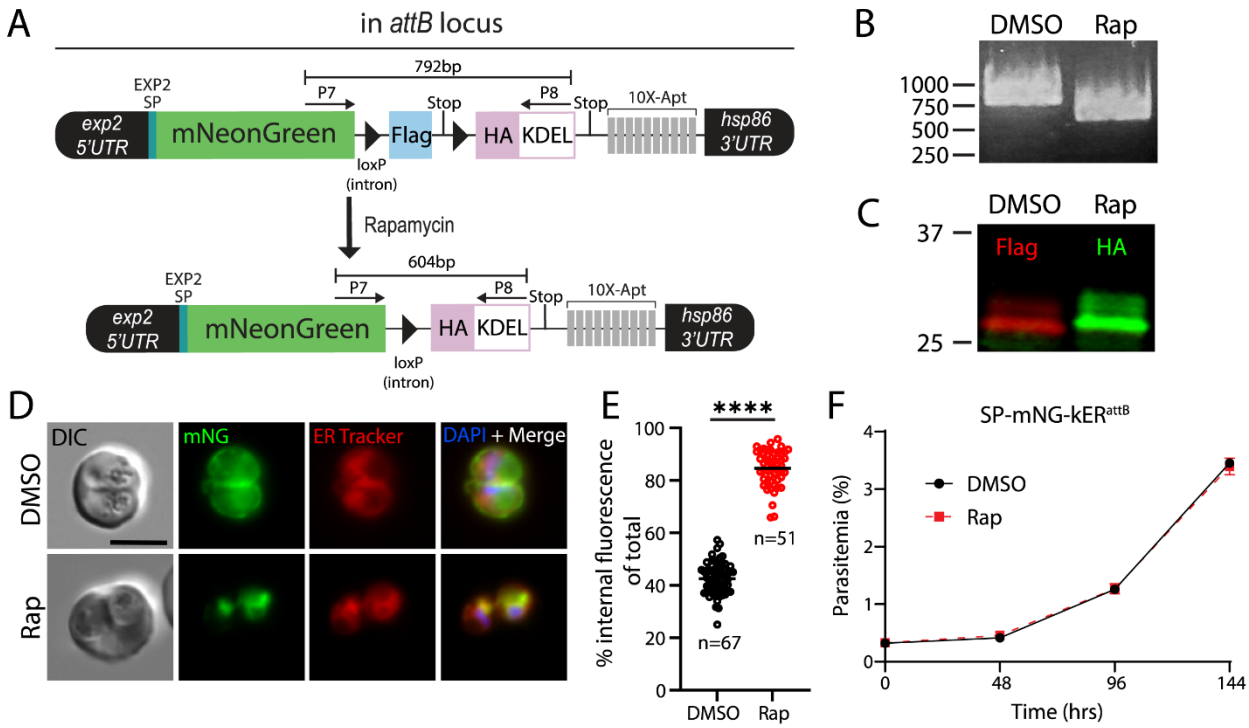

866 **Figure 1. Conditional ER retrieval of a secreted reporter does not impact parasite fitness.**
867 A) Schematic of reporter expression cassette installed at the *attB* site of chromosome 6. An
868 mNeonGreen reporter is fused to the signal peptide of EXP2 and expressed under control of the
869 *exp2* promoter. A 3xFLAG tag and stop codon are flanked by loxP-containing introns (triangles)
870 followed by a 3xHA-KDEL, stop codon and 10X aptamer array. Activation of DiCre by rapamycin
871 treatment excises the FLAG tag, bringing into frame the HA-KDEL tag. B) PCR showing excision
872 in mNG-kER parasites 24hrs after rapamycin treatment using primers P7/8. C) Western blot of
873 reporter 24hrs post treatment with DMSO or rapamycin. Molecular weights after signal peptide
874 cleavage are predicted to be 30.8 kDa for mNG-3xFLAG and 30.9 kDa for mNG-3xHA-KDEL. D)
875 Live microscopy of DMSO or rapamycin-treated parasites 24hrs post-treatment. E) Quantification
876 of percent internal mNG fluorescence 168hrs post-treatment with DMSO or rapamycin. Data are
877 pooled from 2 independent experiments and bar indicates mean (****, P<0.0001; unpaired t test).
878 F) Representative growth of asynchronous parasites (n=2 biological replicates) treated with
879 DMSO or rapamycin. Data are presented as means ± standard deviation from one biological

880 replicate (n = 3 technical replicates). All cultures were maintained in media supplemented with

881 500 nM aTc. Scale bar, 5μm.

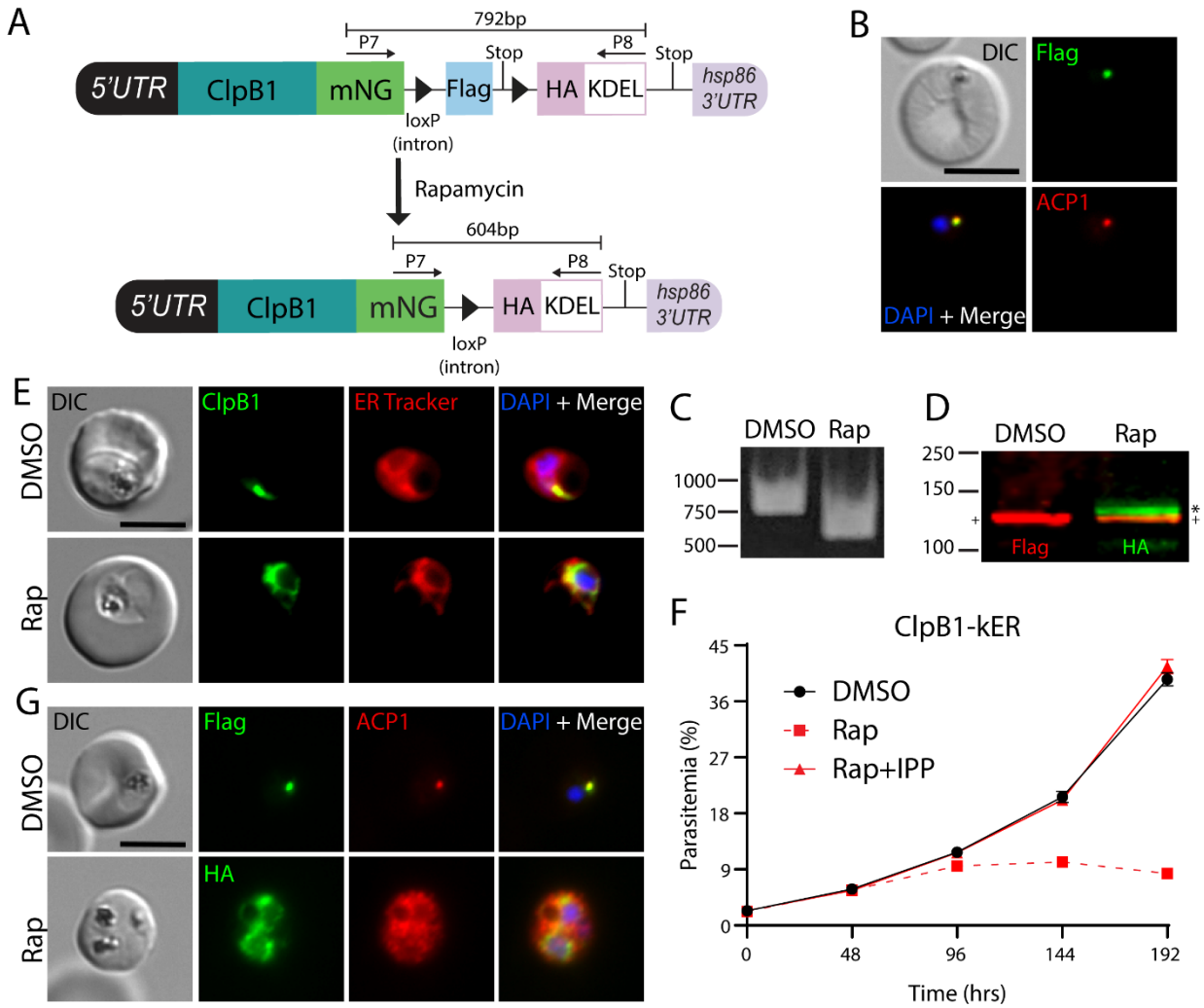

Figure 2. Lethal ER retention of the apicoplast chaperone ClpB1 is rescued by IPP. A) Schematic showing strategy for appending kER to the C-terminus of *clpB1*. B) IFA of PFA fixed parasites stained with mouse anti-Flag and rabbit anti-ACP1 antibodies. C) PCR showing excision in ClpB1-kER parasites 24hrs after rapamycin treatment using primers P7/8. D) Western blot 24hrs post treatment with DMSO or rapamycin. Molecular weights after transit peptide cleavage are predicted to be 135 kDa for ClpB1-mNG-3xFLAG and 135.1 kDa for ClpB1-mNG-3xHA-KDEL. (+) represents the mature form of ClpB1 while the (*) represents ClpB1 with the transit peptide still attached. E) Live microscopy of DMSO or rapamycin-treated parasites 48hrs post-treatment. F) Representative growth of asynchronous parasites (n=3 biological replicates) treated with DMSO or rapamycin, with or without supplementation with 200 μM IPP. Data are presented as

892 means ± standard deviation from one biological replicate (n = 3 technical replicates). G) IFA of
893 PFA fixed parasites stained with mouse anti-Flag or anti-HA and rabbit anti-ACP1 antibodies after
894 3 growth cycles where rapamycin treated parasites were supplemented with 200 μM IPP. Scale
895 bars, 5μm.

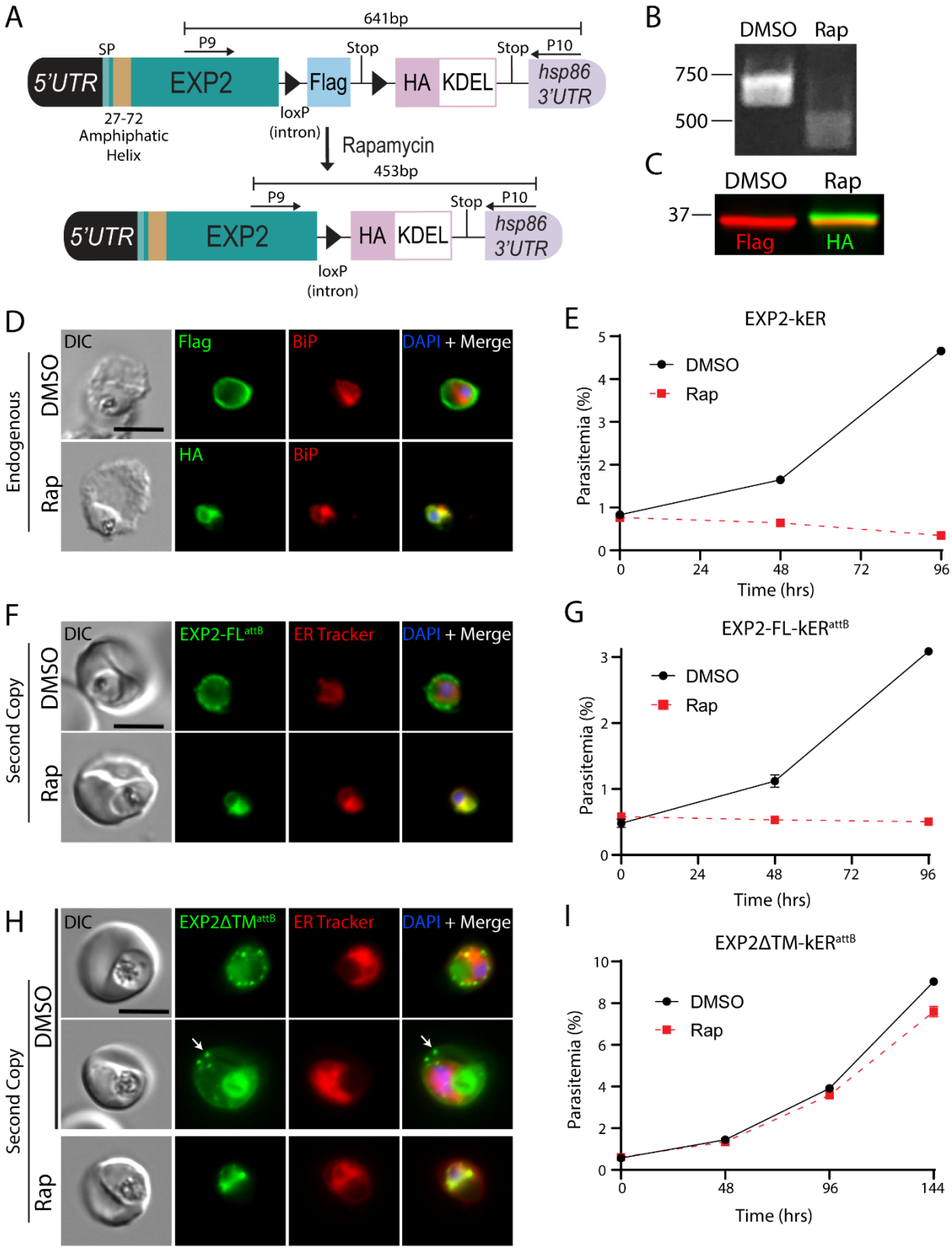

896 **Figure 3. ER retention of EXP2 causes a lethal fitness defect independent of loss of PVM**

897 **transport functions.** A) Schematic showing strategy for appending kER to the endogenous C-

898 terminus of EXP2 without mNG. B) PCR showing excision in EXP2-kER 24hrs after treatment
899 with rapamycin using primers P9/10. C) Western blot of EXP2-kER parasites 24hrs post treatment
900 with DMSO or rapamycin. Molecular weights after signal peptide cleavage are predicted to be
901 34.6 kDa for EXP2-3xFLAG and 34.7 kDa for EXP2-3xHA-KDEL. D) IFA of EXP2-kER 24hrs post-
902 treatment with DMSO or rapamycin. E) Growth of asynchronous parasites (n=2 biological
903 replicates) treated with DMSO or rapamycin. Data are presented as means ± standard deviation
904 from one biological replicate (n = 3 technical replicates). F) Live microscopy of parasites
905 expressing a full-length second copy of EXP2 with an mNG-kER fusion from the *attB* site under
906 the control of the endogenous *exp2* promoter (EXP2-FL-kER^{attB}). Parasites were viewed 24hrs
907 after treatment with DMSO or rapamycin. G) Representative growth of asynchronous EXP2-FL-
908 kER^{attB} parasites (n=2 biological replicates) treated with DMSO or rapamycin. Data are presented
909 as means ± standard deviation from one biological replicate (n = 3 technical replicates). H) Live
910 microscopy of parasites expressing a second copy of EXP2 with mNG-kER fusion and lacking
911 the amphipathic helix from the *attB* site (EXP2ΔTM-kER^{attB}). Parasites were viewed 24hrs after
912 treatment with DMSO or rapamycin. Two representative examples of unexcised parasites are
913 presented, showing localization of the ΔTM version of EXP2 to the PV and host cell in some
914 infected RBCs (arrow). Digestive vacuole fluorescence was also observed as is typical for PV
915 proteins. I) Representative growth of asynchronous EXP2ΔTM-kER^{attB} parasites (n=2 biological
916 replicates) treated with DMSO or rapamycin. Data are presented as means ± standard deviation
917 from one biological replicate (n = 3 technical replicates). Scale bars, 5μm.

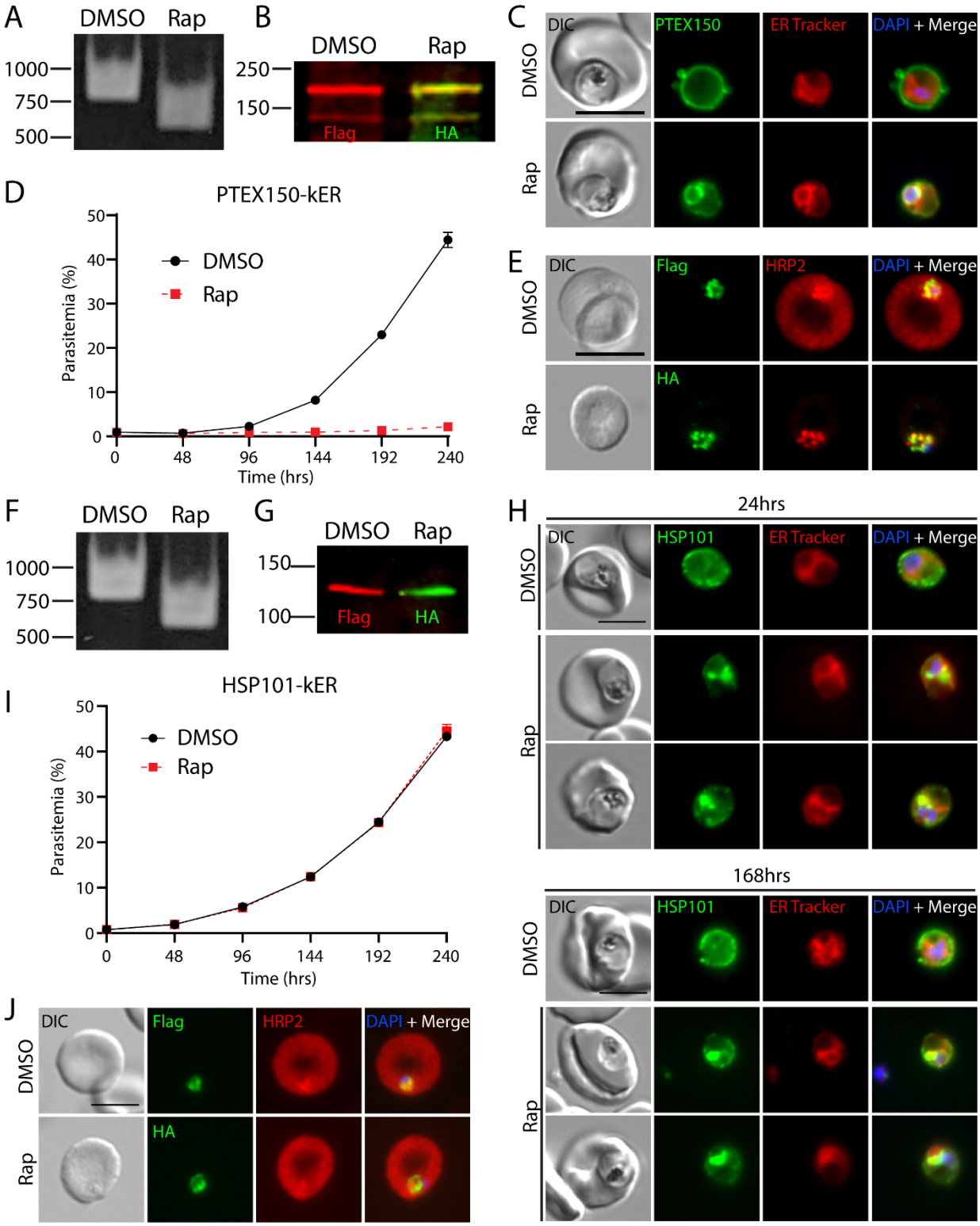

Figure 4. ER retention of PTEX150 but not HSP101 causes a lethal block in protein export *in vitro*. A) PCR showing excision in PTEX150-kER parasites 24hrs after rapamycin treatment using primers P7/8. B) Western blot of PTEX150-kER 24hrs post-treatment with DMSO or

921 rapamycin. Molecular weights after signal peptide cleavage are predicted to be 141 kDa for
922 PTEX150-mNG-3xFLAG and 141.1 kDa for PTEX150-mNG-3xHA-KDEL. Note that PTEX150 is
923 observed to migrate at higher molecular weight than predicted (60). C) Live microscopy of
924 PTEX150-kER 24hrs post-treatment with DMSO or rapamycin-treated. D) Representative growth
925 of asynchronous PTEX150-kER parasites (n=3 biological replicates) treated with DMSO or
926 rapamycin. Data are presented as means ± standard deviation from one biological replicate (n = 3
927 technical replicates). E) IFA of synchronized, ring-stage PTEX150-kER parasites 48hrs post-
928 treatment with DMSO or rapamycin and probed with anti-HRP2 and anti-FLAG or anti-HA
929 antibodies. F) PCR showing excision in HSP101-kER parasites 24hrs after rapamycin treatment
930 using primers P7/8. G) Western blot of HSP101-kER parasites 14 days post-treatment with DMSO
931 or rapamycin. Molecular weights after signal peptide cleavage are predicted to be 130.5 kDa for
932 HSP101-mNG-3xFLAG and 130.6 kDa for HSP101-mNG-3xHA-KDEL. H) Live microscopy of
933 HSP101-kER 24hrs and 168hrs post-treatment with DMSO or rapamycin. I) Representative
934 growth of asynchronous HSP101-kER parasites (n=3 biological replicates) treated with DMSO or
935 rapamycin. Data are presented as means ± standard deviation from one biological replicate (n = 3
936 technical replicates). J) IFA of synchronized, ring-stage HSP101-kER parasites 48hrs post-
937 treatment with DMSO or rapamycin and probed with anti-HRP2 and anti-FLAG or anti-HA
938 antibodies. Scale bar, 5μm.

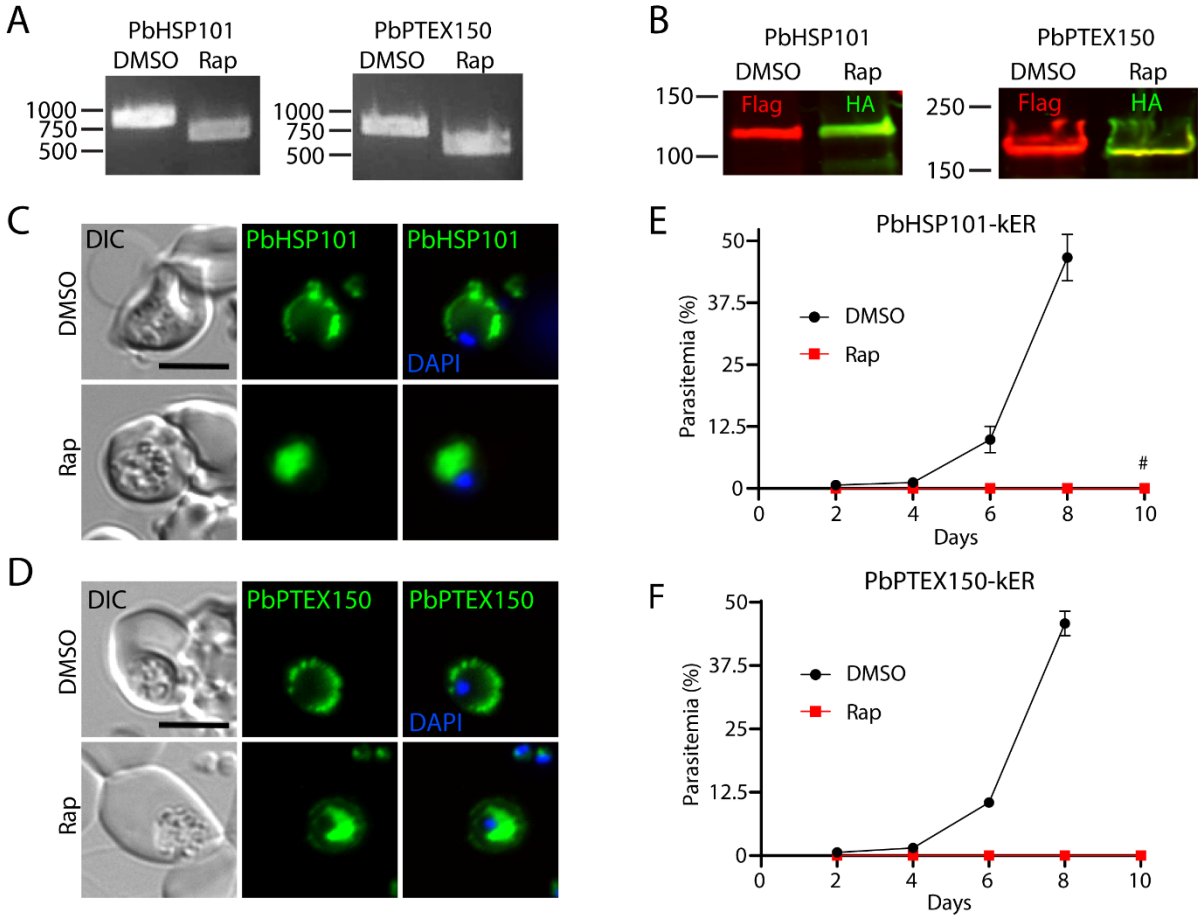

Figure 5: ER retention of HSP101 is lethal *in vivo*. A) PCR showing excision in PbPTEX150-kER and PbHSP101-kER *P. berghei* parasites treated with rapamycin and cultured 18hrs *ex vivo* using primers P7/P60. B) Western blot of PbPTEX150-kER and PbHSP101-kER parasites 24hrs post-treatment with DMSO or rapamycin. Molecular weights after signal peptide cleavage are predicted to be 130.9 kDa for PbHSP101-mNG-3xFLAG, 131 kDa for PbHSP101-mNG-3xHA-KDEL, 130.5 kDa for PbPTEX150-mNG-3xFLAG and 130.6 kDa for PbPTEX150-mNG-3xHA-KDEL. Note that PbPTEX150 is observed to migrate at higher molecular weight than predicted (99). C,D) Live microscopy of PbHSP101-kER or PbPTEX150-kER parasites 18hrs post-treatment with DMSO or rapamycin. E,F) Parasitemia of PbHSP101-kER or PbPTEX150-kER infected mice inoculated by tail vein-injection of parasites treated *ex vivo* with DMSO or rapamycin. Data are presented as means ± standard deviation of three independent experiments (one mouse infected per treatment in each experiment). No parasites were observed in mice

951 injected with rapamycin treated parasites except that one mouse injected with rapamycin-treated
952 PbHSP101-kER parasites became patent on day 10 (#). However, PCR showed these parasites
953 had not undergone excision (see Figure S6B). Scale bars, 5μm.

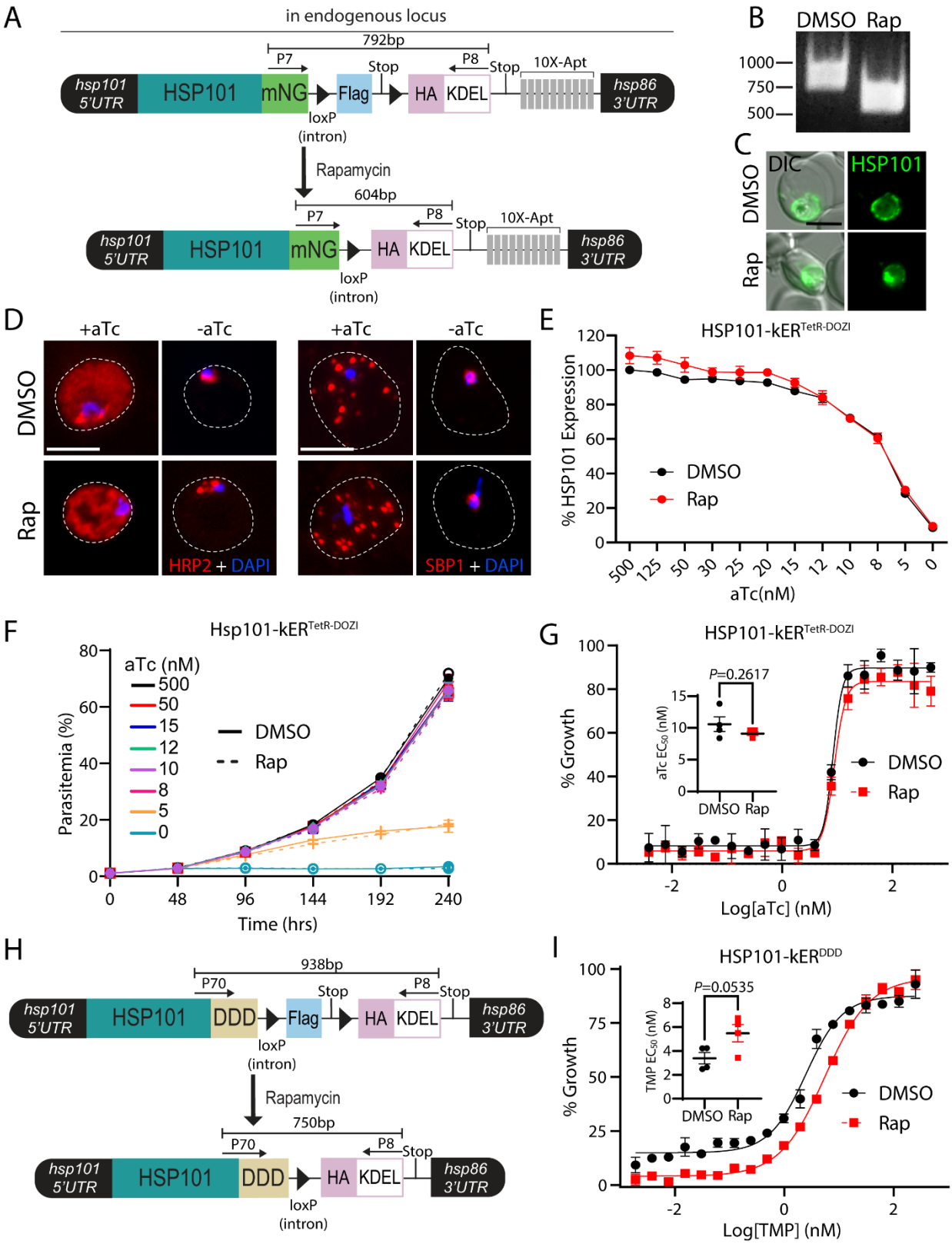

954 **Figure 6. Depletion of HSP101 PV levels hypersensitizes parasites to post-translational**

955 **destabilization of the HSP101-PTEX complex but not HSP101 translational knockdown.** A)

956 Schematic showing strategy for appending kER and the TetR-DOZI aptamers system to the
957 endogenous C-terminus of HSP101. B) PCR showing excision in HSP101-kER$^{TetR-DOZI}$ parasites
958 24hrs after rapamycin treatment using primers P7/8. C) Live microscopy of HSP101-kER$^{TetR-DOZI}$
959 parasites 168hrs post-treatment with DMSO or rapamycin. D) IFA detecting the soluble PEXEL
960 protein HRP2 or the transmembrane PNEP SBP1 in synchronized, ring-stage HSP101-kER^{TetR-}
961 ^{DOZI} parasites grown for 48hrs +/- aTc and treated with DMSO or rapamycin 1 cycle prior. E)
962 Quantification of HSP101 levels by flow cytometry measurement of mNeonGreen fluorescence in
963 HSP101-kER$^{TetR-DOZI}$ parasites grown for 48 hrs at indicated aTc concentrations and treated with
964 DMSO or rapamycin 2 cycles prior. MFI data were normalized to DMSO-treated parasites grown
965 in 500 nM aTc (100%) and presented as mean ± SEM (n = 5 biological replicates). F)
966 Representative growth curves (n = 4 biological replicates) of HSP101-kER$^{TetR-DOZI}$ parasites grown
967 at indicated aTc concentrations and treated with DMSO or rapamycin 2 cycles prior. Data are
968 presented as means ± standard deviation from one biological replicate (n = 3 technical replicates).
969 G) Representative EC_{50} shift assay (n=4 biological replicates) of parasites treated with DMSO or
970 rapamycin with two-fold dilutions of aTc starting at 500nM. Data are presented as means ±
971 standard deviation from one biological replicate (n = 3 technical replicates). EC_{50} graph inset
972 presented as mean ± SEM (n = 4 biological replicates): DMSO=10.58±1.16 nM and
973 rapamycin=9.11±0.29 nM. H) Schematic showing strategy for appending kER and the DDD
974 system to the endogenous C-terminus of HSP101. I) Representative EC_{50} shift assay (n=4
975 biological replicates) of parasites treated with DMSO or rapamycin with two-fold dilutions of TMP
976 starting at 250nM. Data are presented as means ± standard deviation from one biological replicate
977 (n = 3 technical replicates). EC_{50} graph inset presented as mean ± SEM (n = 4 biological
978 replicates): DMSO=3.39±0.48 nM and rapamycin 5.48±0.73 nM. Scale bars, 5μm.